Nuclear factor E2-related factor 2 deficiency impairs atherosclerotic lesion development but promotes features of plaque instability in hypercholesterolaemic mice

Ruotsalainen, Anna-Kaisa

2019-01-01

Ruotsalainen , A-K , Lappalainen , J P , Heiskanen , E , Merentie , M , Sihvola , V , Näpänkangas , J , Lottonen-Raikaslehto , L , Kansanen , E , Adinolfi , S , Kaarniranta , K , Ylä-Herttuala , S , Jauhiainen , M , Pirinen , E & Levonen , A-L 2019 , ' Nuclear factor E2-related factor 2 deficiency impairs atherosclerotic lesion development but promotes features of plaque instability in hypercholesterolaemic mice ' , Cardiovascular Research , vol. 115 , no. 1 , pp. 243-254 . https://doi.org/10.1093/cvr/cvy143

http://hdl.handle.net/10138/311312
https://doi.org/10.1093/cvr/cvy143

acceptedVersion

Nrf2 deficiency impairs atherosclerotic lesion development but promotes features of plaque instability in hypercholesterolemic mice

Anna-Kaisa Ruotsalainen MSc.[1], Jari P. Lappalainen PhD[1,2], Emmi Heiskanen MD[1], Mari Merentie MD, PhD[1], Virve Sihvola MSc.[1], Juha Näpänkangas MD[3], Line Lottonen-Raikaslehto MD, PhD[1], Emilia Kansanen PhD[1], Simone Adinolfi MSc[1], Kai Kaarniranta MD, PhD[4], Seppo Ylä-Herttuala MD, PhD[1,5], Matti Jauhiainen PhD[6,7], Eija Pirinen PhD[8], Anna-Liisa Levonen MD, PhD[1]

[1]A.I. Virtanen Institute, University of Eastern Finland, Kuopio, Finland
[2]Department of Clinical Chemistry, University of Eastern Finland and Eastern Finland Laboratory Centre, Kuopio, Finland
[3]Department of Pathology, Oulu University Hospital and University of Oulu, Oulu, Finland
[4]Department of Ophthalmology, University of Eastern Finland and Kuopio University Hospital, Kuopio, Finland
[5]Heart Center and Gene Therapy Unit, Kuopio University Hospital, Kuopio, Finland
[6]Minerva Foundation Institute for Medical Research, Helsinki, Finland
[7]National Institute for Health and Welfare, Genomics and Biomarkes Unit, Helsinki, Finland
[8]Research Program for Molecular Neurology, University of Helsinki, Helsinki, Finland

Corresponding author:
Anna-Liisa Levonen, MD, PhD,
A.I.Virtanen Institute
Neulaniementie 2
P.O.Box 1627
70211 Kuopio, Finland
Tel +358 40 358 9907, e-mail: anna-liisa.levonen@uef.fi

Word count: 6998
Number of figures: 7
Number of tables: 3

Abstract

Aims: Oxidative stress and inflammation play an important role in the progression of atherosclerosis. Transcription factor NF-E2-related factor 2 (Nrf2) has antioxidant and anti-inflammatory effects in the vessel wall, but paradoxically, global loss of Nrf2 in apoE deficient mice alleviates atherosclerosis. In this study, we investigated the effect of global Nrf2 deficiency on early and advanced atherogenesis in alternative models of atherosclerosis, LDL receptor deficient mice ($LDLR^{-/-}$) and $LDLR^{-/-}$ mice expressing apoB-100 only ($LDLR^{-/-}ApoB^{100/100}$) having a humanized lipoprotein profile.

Methods and Results: $LDLR^{-/-}$ mice were fed a high fat diet (HFD) for 6 or 12 weeks and $LDLR^{-/-}ApoB^{100/100}$ mice a regular chow diet for 6 or 12 months. Nrf2 deficiency significantly reduced early and more advanced atherosclerosis assessed by lesion size and coverage in the aorta in both models. Nrf2 deficiency in $LDLR^{-/-}$ mice reduced total plasma cholesterol after 6 weeks of HFD and triglycerides in $LDLR^{-/-}ApoB^{100/100}$ mice on a chow diet. Nrf2 deficiency aggravated aortic plaque maturation in aged $LDLR^{-/-}ApoB^{100/100}$ mice as it increased plaque calcification. Moreover, approximately 36% of $Nrf2^{-/-}LDLR^{-/-}ApoB^{100/100}$ females developed spontaneous myocardial infarction or sudden death at 5 to 12 months of age. Interestingly, Nrf2 deficiency increased plaque instability index, enhanced plaque inflammation and calcification, and reduced fibrous cap thickness in brachiocephalic arteries of $LDLR^{-/-}ApoB^{100/100}$ female mice at age of 12 months.

Conclusion(s): Absence of Nrf2 reduced atherosclerotic lesion size in both atherosclerosis models, likely via systemic effects on lipid metabolism. However, Nrf2 deficiency in aged $LDLR^{-/-}ApoB^{100/100}$ mice led to an enhanced atherosclerotic plaque instability likely via increased plaque inflammation and oxidative stress, which possibly predisposed to myocardial infarction and sudden death.

Keywords: Nrf2, oxidative stress, inflammation, atherosclerosis, plaque phenotype

Introduction

Atherosclerosis is a chronic inflammatory disease within the intima of large and medium-sized arteries. Accumulation of lipids and an ensuing persistent inflammatory response leads to a gradual formation of atherosclerotic plaques, which ultimately develop to complex lesions[1]. The stability of lesions is a critical factor affecting the development of complications. Advanced fibroatheroma plaques that have large necrotic core and thin fibrous cap with infiltrated inflammatory cells in the shoulder region are unstable and prone to rupture, predisposing to myocardial infarction, stroke and sudden death[2,3].

Oxidative stress, an imbalance between the production and disposal of reactive oxygen species (ROS), contributes to atherogenesis and formation of unstable atherosclerotic lesions[4]. Low-density lipoprotein (LDL) particles entrapped in the arterial intima are modified by ROS, evoking activation of macrophages, endothelial cells and smooth muscle cells to produce pro-inflammatory cytokines, leading to atherosclerotic lesion progression and chronic inflammation[5,6]. The balance between the formation and disposal of ROS is maintained by antioxidant genes that can be regulated in an integrated manner by the transcription factor Nuclear factor E2-related factor 2 (Nrf2), which is responsive to both environmental factors and endogenous stimuli. Nrf2 is ubiquitously expressed in vascular cells, and it regulates several antioxidant enzymes providing cytoprotection in the vasculature. Many of them, such as heme oxygenase-1, glutathione reductase, and peroxiredoxin-1 and -2, have been shown to be atheroprotective in atherosclerotic mouse models[7,8,9,10]. Nrf2 regulates antioxidant gene expression in vascular cells after exposure to modified LDL[11] and oxidized phospholipids *in vivo*[12] in the carotid artery, and it is activated by laminar shear stress *in vitro*[13] as well as *in vivo*[14]. Adenoviral Nrf2 gene transfer inhibits vascular inflammation and oxidative stress in a rabbit angioplasty model[15]. Moreover, Nrf2 deficiency in bone marrow derived macrophages aggravates atherosclerosis in $LDLR^{-/-}$ mice, supporting the notion that Nrf2 is atheroprotective in the vascular wall[16,17].

Contradictory to the antioxidant and anti-inflammatory effects of Nrf2, global Nrf2 deficiency alleviates atherosclerosis in hypercholesterolemic $ApoE^{-/-}$ mice[18,19,20,21]. The mechanisms by which Nrf2 mediates its proatherogenic action in this model is currently unknown, but combined systemic and local vascular effects have been suggested. Nrf2 deficiency has been shown to decrease plasma total cholesterol on a regular chow or on a high-fat diet (HFD) in $ApoE^{-/-}$ mice in some[19,20] but not in all studies[18,21]. $ApoE^{-/-}$ mice are widely used in the field of atherosclerosis research, but their plasma lipoprotein profiles only poorly recapitulate that of human hypercholesterolemia. $ApoE^{-/-}$ mice have certain shortcomings in modeling human atherosclerosis as they have a non-physiological lipoprotein profile consisting mainly of VLDL and chylomicron remnants that have apoB-48 as the major apolipoprotein. Moreover, apoE has direct functions in the vessel wall as it facilitates cholesterol efflux from macrophage foam cells, and directly modifies macrophage- and T lymphocyte-mediated immune responses thereby affecting vascular inflammation[22,23,24,25]. In the $LDLR^{-/-}ApoB^{100/100}$ mouse model, the apoB-100 mRNA tissue-specific RNA editing is blocked and only apoB-100 protein is produced resulting in a more human-like hypercholesterolemia even on a regular chow diet[26,27,28]. $LDLR^{-/-}$ mice on the other hand exhibit only a modest increase in plasma LDL cholesterol on a regular chow diet and they do not develop significant lesions unless fed HFD[29].

Nrf2 has protective functions via regulation of antioxidant and anti-inflammatory genes, and thus it is a promising drug target for the treatment of chronic inflammatory diseases. Given that oxidative stress and inflammation has been implicated to play a pivotal role also in the development of atherosclerotic lesions, we postulated that Nrf2 would be protective against atherosclerosis. As the role of Nrf2 in atherogenesis and plaque composition has remained unclear, we aimed to investigate the effect of global Nrf2 deficiency on the development of atherosclerotic lesions, plaque phenotype and circulating lipid levels using two different mouse

models, which mimic more closely human hypercholesterolemia and atherogenesis in comparison to ApoE$^{-/-}$ mice[29]. Interestingly, our results show that Nrf2 deficiency retards atherosclerotic lesion development determined by reduced plaque size in both HFD fed LDLR$^{-/-}$ mice as well as in aged chow-fed LDLR$^{-/-}$ApoB$^{100/100}$ mice. However, Nrf2 deficient mice in LDLR$^{-/-}$ApoB$^{100/100}$ background show signs of plaque instability likely via enhanced atheroma plaque inflammation and oxidative stress that may predispose to spontaneous myocardial infarction in female LDLR$^{-/-}$ApoB$^{100/100}$ mice as well.

Methods

Animals

Nrf2-deficient (Nrf2$^{-/-}$) mice (C57Bl/6J background, a kind gift from Masayuki Yamamoto, Tohoku University, Sendai) were cross-bred with LDLR$^{-/-}$ (C57Bl/6J background, backcrossed ten times, The Jackson Laboratory, Bar Harbor, ME, USA) and LDLR$^{-/-}$ApoB$^{100/100}$ mice (129sv/B6 mixed background, backcrossed ten times, The Jackson Laboratory, Bar Harbor, ME, USA) to obtain Nrf2$^{-/-}$LDLR$^{-/-}$ and Nrf2$^{-/-}$LDLR$^{-/-}$ApoB$^{100/100}$ mice. Three-month-old male and female LDLR$^{-/-}$ and their littermate Nrf2$^{-/-}$LDLR$^{-/-}$ mice were fed HFD (TD88137, Harlan Teklad: 42 % of calories from fat and 0.15 % cholesterol) for 6 or 12 weeks. Female and male LDLR$^{-/-}$ApoB$^{100/100}$ and their littermate Nrf2$^{-/-}$LDLR$^{-/-}$ApoB$^{100/100}$ mice were fed a regular chow diet (Teklad Global 16 % Protein Rodent Diet: 12 % of calories from fat and 0 % cholesterol) until the age of 6 or 12 months. Mice were housed in the Animal Centre of University of Eastern Finland in controlled conditions for temperature and humidity, using a 12 h light/dark cycle and had an *ad libitum* access to food and water. All animal experiments were approved by the National Experimental Animal Board of Finland and carried out following the guidelines of the Finnish Act on Animal Experimentation and directive 2010/63/EU of the European Parliament.

Measurements of atherosclerosis and plaque morphology

The mice were euthanized by CO_2 inhalation and perfused with phosphate buffered saline. For analysis of atherosclerosis, aortic root and brachiocephalic arteries were fixed in 4% paraformaldehyde (pH 7.4). Tissues were embedded in paraffin for serial cross-sectional analysis (5 µm sections, mean of 3 sections per mouse at 25 µm intervals), excluding aortas, which were prepared for *en face* analysis and stained with Oil Red O.

Cross sections of aortic root and brachiocephalic arteries were stained with hematoxylin-eosin to quantify the average lesion area (mean of 5 sections per mouse at 25 µm intervals), which were measured with a color image analysis system (analySIS 3.00 Software). For the analysis of macrophages in the aortic and brachiocephalic lesions, serial sections from the aortic root and brachiocephalic artery were selected, immunostained with mMQ (anti mouse macrophage, mMQ AIA31240, 1:6500, Accurate Chemical & Scientific Corp.) and positive areas were quantified with a color image analysis system (analySIS 3.00 Software). For the analysis of smooth muscle cells in the brachiocephalic lesions, serial sections from brachiocephalic artery were stained with a αSMA (anti-alpha smooth muscle actin, ab15267, Abcam) and SMHC (anti-smooth muscle myosin heavy chain, ab53219, Abcam) primary antibodies and positive areas were measured. In addition, brachiocephalic artery sections were stained with a MCP-1 (rabbit-anti mouse, ab7020, Abcam) and TNFα (rabbit-anti mouse, ab6671, Abcam) primary antibody to measure plaque inflammation, and with 4-hydroxynonenal (4-HNE) (rabbit-anti mouse, LS-C68182, LSBio) and anti-nitrotyrosine (3-NT) primary antibody (rabbit-anti mouse, 06-284, Merck Millipore) as a measure of oxidative stress.

Aortic plaque necrosis was measured from hematoxylin and eosin stained sections and brachiocephalic artery necrosis from Masson trichrome stained sections. Plaque necrosis was measured by morphological criteria in which plaque cholesterol clefts, lipid droplets and acellular areas were regarded as necrotic areas. Moreover, to quantify fibrous cap thickness from brachiocephalic arteries, three serial sections per mouse were stained with Masson´s Trichrome. In every section, three to five of the thinnest caps were selected and the average was calculated. All the previous measurements were done with a color image analysis system (analySIS 3.00 Software). Furthermore, fibrous cap thickness was analyzed in relation to necrotic core area to measure cap to core ration (mm/mm^2). In addition, to analyze plaque calcification, aortic and brachiocephalic sections were stained with Alizarin Red S, which stains calcific depositions with red color, which was quantified. Brachiocephalic sections were stained with Movat Pentachrome, which stains elastic and reticular fibers, collagen and mucin, to detect fibro fatty nodule area with the color image analysis system (analySIS 3.00 Software). Moreover, to detect brachiocephalic plaque collagen content, arterial cross sections were stained with Sirius Red S protocol and collagen was quantified with the Image J 1.48V Software based on threshold and represented in relation to total plaque area. Finally, macrophage area, necrotic area, collagen content and smooth muscle cell content were used to measure plaque instability index from brachiocephalic artery plaques as follows: (macrophages% + necrotic area%)/(collagen% + smooth muscle cells%)=instability index[30,31,32]. Quantification of plaque morphology was done in relation to total plaque area with Image J 1.48V Software based on threshold unless otherwise stated. All analyses were done in a blinded manner.

Analysis of body fat composition

Organ weights were determined for 6-month-old female $LDLR^{-/-}ApoB^{100/100}$ (n=4) and $Nrf2^{-/-}LDLR^{-/-}ApoB^{100/100}$ (n=4) mice. The fat fraction of the mice was determined from $LDLR^{-/-}ApoB^{100/100}$ (n=4) and $Nrf2^{-/-}LDLR^{-/-}ApoB^{100/100}$ (n=4) female mice at the age of 6 months using magnetic resonance imaging. For the imaging, the mice were anesthetized with isoflurane inhalation (4% for induction and approximately 1.5% during imaging). The mouse was placed on a holder and a pneumatic pillow was placed under the mouse for respiration monitoring and gating. A 9.4 T horizontal scanner equipped with Agilent Direct Drive console (Agilent Corp., Palo Alto, CA, USA) with a quadrature volume coil with inner diameter 63 mm (Varian, Palo Alto, CA, USA) was used for transmitting and receiving the imaging signal. A 3D chemical-shift-selective gradient echo sequence with respiration gating was used to acquire interleaved fat and water images used for calculation of the fat quantity as previously described[33]. Parameters used for imaging were: repetition time = 70 ms, echo time = 4.2 ms, field of view = 80 x 40 x 40 mm3, and matrix size = 256 x 64 x 64 with 2 averages.

Analysis of plasma lipid profile and inflammatory cytokines

After an overnight 12 h fasting-period, approximately 100 µl blood was drawn from the saphenous vein of $LDLR^{-/-}$ and $Nrf2^{-/-}LDLR^{-/-}$ male and female mice before and after HFD and from $LDLR^{-/-}ApoB^{100/100}$ and $Nrf2^{-/-}LDLR^{-/-}ApoB^{100/100}$ female and male mice at the age of 6 or 12 months on a regular chow diet. Plasma was isolated by centrifugation at 4 °C, 1700 × g for 15 min and stored at −80 °C for further analysis. Plasma triglycerides were analyzed using the Triglycerides GPO-PAP-kit (Roche Diagnostics), total cholesterol using the Cholesterol CHOD-PAP kit (Roche Diagnostics). Plasma –pro-inflammatory cytokines were analyzed using BD™ Cytometric Bead Array (CBA) kit according to the manufacturer's instructions. The samples were run on FACS Calibur flow cytometer (BD Biosciences) and the results were analyzed using FCAP Array 2.0.0 software (Soft Flow Hungary Ltd, Pecs, Hungary).

Echocardiography

Echocardiography was performed for LDLR$^{-/-}$ApoB$^{100/100}$ (n=4) and Nrf2$^{-/-}$LDLR$^{-/-}$ApoB$^{100/100}$ (n=7) female mice at the age of 6 using Vevo® 2100 Ultrasound System (Fujifilm Visual Sonics ®). In brief, mice were kept fully anesthesized with 2% isoflurane inhalation. Heart rates were approximately 500 bpm in controls and in atherosclerotic mice. Standard M-mode measurements of the left ventricle dimensions, left ventricle mass and volume, ejection fraction (calculated with Teicholz formula) and stroke volume were measured in parasternal short-axis view as described earlier in [34]

Isolation of bone marrow derived macrophages

Nrf2$^{-/-}$LDLR$^{-/-}$ApoB$^{100/100}$ and LDLR$^{-/-}$ApoB$^{100/100}$ mice were euthanized by CO_2 inhalation. Femoral and tibial bones were dissected and all the remaining tissue on the bones was removed. Each bone end was cut off, and bone marrow was expelled by flushing with ice cold PBS. Cells were cultured for 7 days in RPMI1640 medium with 10% fetal bovine serum (FBS), 1% Penicillin-Streptomycin (P/S) and 20 ng/ml macrophage colony stimulating factor (M-CSF, Miltenyi Biotec®) on 10 cm Petri dishs, at 37°C. Medium was changed every third day. Matured macrophages (5-10×10^6/dish) were harvested by trypsin-EDTA (0.25%).

Gene expression analysis

Bone marrow derived macrophages were cultured on 6-well plates and starved for 4 hours in Optimem (Gibco®) with 10% LPDS and 1% P/S, then they were incubated for further 16 hours at + 37˚C either in the absence or presence of acetylated LDL (AcLDL) (50 µg protein/ml) or LPS from *Escherichia coli* (Sigma-Aldrich® 10 ng/ml). RNA was extracted by using NucleoZOL® (Macherey-Nagel) and 500 ng of total RNA was reverse transcribed into cDNA using Transcriptor First Strand cDNA Synthesis Kit (REF04897030001, Roche). Quantitative measurements of gene expression were performed using the Light Cycler 96 Real-Time PCR System (Roche), appropriate Universal ProbeLibrary (UPL) products from Roche and the following primers from Sigma Aldrich: 5´-catccacgtgttggctca-3´ and 5´-gatcatcttgctggtgaatgagt-3´ (UPL 62) for MCP-1, 5´-ctgtagcccacgtcgtagc-3´ and 5´-ttgagatccatgccgttg-3´ (UPL 25) for TNF-α, 5´-agttgacggaccccaaaag-3´ and 5´-agctggatgctctcatcagg-3´ (UPL 38) for IL-1β, 5´-gctaccaaactggatataatcagga-3´ and 5´-gctaccaaactggatataatcagga-3´ and 5´-ccaggtagctatggtactccagaa-3´ (UPL 6) for IL-6. Measurements were done as 3-6 samples measured. The expression levels were normalized to β_2-microglobulin expression (Applied Biosystems TaqMan Gene Expression Assays Mm00437762_m1) and the data are presented as fold change in the expression *versus* control.

Statistical Analyses

Data normal distribution was tested by the Shapiro-Wilk test and to evaluate statistical significance ($p<0.05$), unpaired two tailed Student's *t*-test or Log-rank test were used. Numerical values for each measurement are shown as mean ± SEM. All statistical analyses were performed using GraphPad Prism® (GraphPad 5.03 Software).

Results

Nrf2 deficiency impairs development of diet-induced atherosclerosis in LDLR$^{-/-}$ male and female mice

To determine the role of Nrf2 in atherogenesis, mice lacking Nrf2 in atherosclerosis-prone LDLR$^{-/-}$ background were subjected to a HFD for 6 or 12 wk to generate early foam cell-rich and more advanced atherosclerotic plaques, respectively.[29] Nrf2$^{-/-}$LDLR$^{-/-}$ male mice had ~50% and ~30% smaller atherosclerotic lesions in aortic root than LDLR$^{-/-}$ mice after 6 wk and 12 wk of HFD, respectively (Figure 1A). In addition, the lesion area of the entire aorta was reduced in Nrf2$^{-/-}$LDLR$^{-/-}$ male mice after 12 wk of HFD (Figure 1B). In females, the effect was less pronounced, as the difference of the cross sectional lesion area between LDLR$^{-/-}$ and Nrf2$^{-/-}$LDLR$^{-/-}$ mice was significant only after 12 wk of HFD (Figure IA-B in the online-only Data Supplement).

Characterization of plaque morphology of aortic root showed that lesions of both LDLR$^{-/-}$ and Nrf2$^{-/-}$LDLR$^{-/-}$ mice consisted almost entirely of macrophages after 6 wk of HFD, but the macrophage positive area normalized to lesion area remained high only in Nrf2$^{-/-}$LDLR$^{-/-}$ mice after 12 wk of HFD (Figure 2A). In addition, the relative size of the necrotic core of the plaque area was decreased by ~50% in Nrf2$^{-/-}$LDLR$^{-/-}$ mice compared to LDLR$^{-/-}$ mice after 12 wk HFD (Figure 2B). In Nrf2$^{-/-}$LDLR$^{-/-}$ mice, lesions were foam cell-rich early atheromas (type I-II)[35], but in LDLR$^{-/-}$ mice lesions contained small necrotic areas and cholesterol crystals in the lesion core as well as macrophage accumulation in the shoulder area (type II-III) (Figure 2A-B)[35]. These results support the notion that total loss of Nrf2 delays HFD-induced lesion progression in LDLR$^{-/-}$ mice.

Nrf2 deficiency impairs the development of ageing-induced atherosclerosis but promotes plaque necrosis and calcification in LDLR$^{-/-}$ApoB$^{100/100}$ female mice

To investigate the effect of Nrf2 deficiency on atherosclerosis without added dietary fat, we analysed vascular samples from aged LDLR$^{-/-}$ApoB$^{100/100}$ mice that develop more mature and complex lesion morphology compared to LDLR$^{-/-}$ mice.[36] Nrf2 deficiency did not have an effect on aortic root lesion area in male LDLR$^{-/-}$ApoB$^{100/100}$ mice at the age of 6 or 12 months (Figure IIA in the online-only Data Supplement). However, the aortic root lesion area was reduced by ~30% in female Nrf2$^{-/-}$LDLR$^{-/-}$ApoB$^{100/100}$ mice at the age of 6 months (Figure 3A). After 12 months, the loss of Nrf2 decreased the lesional coverage by ~65% in *en face*-analysis of descending aortas (Figure 3B), whereas the difference between the two groups was not statistically significant at the level of aortic root (Figure 3A).

Due to the gender difference in atherogenesis in LDLR$^{-/-}$ApoB$^{100/100}$ vs. Nrf2$^{-/-}$LDLR$^{-/-}$ApoB$^{100/100}$ mice, we chose to examine the plaque morphology more closely in female mice. Notably, atherosclerotic lesions were very complex in both LDLR$^{-/-}$ApoB$^{100/100}$ and Nrf2$^{-/-}$LDLR$^{-/-}$ApoB$^{100/100}$ mice at the age of 6 months, containing necrotic and amorphous areas, fibrosis and varying thickness of smooth muscle cell cap covering the necrotic core. Characterization of plaque composition showed that macrophage positive area relative to lesion area was equal in both groups at the age of 6 and 12 months (Figure 4A). However, the necrotic core area was increased by ~90% in Nrf2$^{-/-}$LDLR$^{-/-}$ApoB$^{100/100}$ mice at the age of 6 months compared to LDLR$^{-/-}$ApoB$^{100/100}$ mice (Figure 4B). Plaques were highly acellular in both groups at the age of 12 months. In Nrf2$^{-/-}$LDLR$^{-/-}$ApoB$^{100/100}$ mice the size of necrotic core in relation to total lesion area was smaller (Figure 4B) but showed increased plaque calcification (~330%) in comparison to LDLR$^{-/-}$ApoB$^{100/100}$ mice at the age of 12 months (Figure 4C). There was no measurable calcification in aortic root plaques at the age of 6 months (Figure IIB in the online-only Data Supplement). Moreover, Nrf2 deficiency increased positive staining area of 4-HNE, an aldehyde

produced during lipid peroxidation that reflects ROS generation at the age of 6 months (Figure 4D).

Nrf2 deficiency lowers plasma total cholesterol in LDLR$^{-/-}$ male mice and plasma triglycerides in LDLR$^{-/-}$ApoB$^{100/100}$ female mice

HFD increased the body weight in all groups, but Nrf2$^{-/-}$LDLR$^{-/-}$ mice were protected from HFD induced obesity, when compared to LDLR$^{-/-}$ mice (Table 1). Nrf2-deficiency reduced body weight also in LDLR$^{-/-}$ApoB$^{100/100}$ females at the age of 6 months on a regular chow diet (Table 2). In addition, the body fat content and amount of epididymal fat were reduced in Nrf2$^{-/-}$LDLR$^{-/-}$ ApoB$^{100/100}$ female mice in comparison to LDLR$^{-/-}$ApoB$^{100/100}$ females at the age of 6 months on a chow diet (Figure IIIA-B in the online-only Data Supplement). Supporting systemic effects on lipid metabolism, Nrf2 deficiency significantly reduced plasma total cholesterol after 6 weeks of HFD in LDLR$^{-/-}$ mice, but the difference disappeared after 12 wk of HFD (Table 1). Nrf2 deficiency did not change plasma triglycerides after 6 wk of HFD, but there was a significant increase after 12 wk of HFD in Nrf2$^{-/-}$LDLR$^{-/-}$ mice. Plasma total cholesterol and triglyceride levels did not differ between the genotypes in female LDLR$^{-/-}$ mice. (Table 1). In LDLR$^{-/-}$ ApoB$^{100/100}$ females, Nrf2 deficiency had no effect on plasma total cholesterol, but it reduced plasma triglycerides significantly by ~20% at both 6 and 12 months of age (Table 2). However, Nrf2$^{-/-}$LDLR$^{-/-}$ApoB$^{100/100}$ males had lower plasma total cholesterol at the age of 12 months in comparison to LDLR$^{-/-}$ ApoB$^{100/100}$ males, but triglyceride levels did not differ between the genotypes at any age in males (Table 2).

Nrf2 deficiency predisposes to myocardial infarction and sudden death in LDLR$^{-/-}$ ApoB$^{100/100}$ female mice

As LDLR$^{-/-}$ApoB$^{100/100}$ (n=44) and Nrf2$^{-/-}$LDLR$^{-/-}$ApoB$^{100/100}$ (n=53) female mice were aged for atherosclerosis experiments, we observed that ~36% of the Nrf2-deficient female mice (19/53) displayed weakness to an extent that required the mice be euthanized or died suddenly between the age of 5 to 12 months ($p<0.05$) (Figure 5A). The mice in a weak condition showed variable symptoms, such as remarkable lowering in body weight (30-45% reduction), hypothermia, dyspnea or lower consciousness. Post mortem dissection revealed spontaneous MIs (10/53) with respective dilation of the heart ventricles and pulmonary edema ($p<0.05$ in comparison to LDLR$^{-/-}$ApoB$^{100/100}$ female mice) (Figure 5A). While in most cases mice died suddenly or had to be euthanized for ethical reasons without further study, we were able to image myocardial infarction by echocardiography from a Nrf2$^{-/-}$LDLR$^{-/-}$ApoB$^{100/100}$ female mouse. Echocardiographic imaging showed dilated left ventricle as well as apical wall thinning and akinesis. In addition, the ejection fraction was markedly decreased (Supplemental video). Histopathological examination revealed coronary atherosclerosis (Figure 5B) and varied sizes of infarcted areas in the left ventricle anterior wall with myocardial dilation (Figure 5C). One of the Nrf2$^{-/-}$LDLR$^{-/-}$ApoB$^{100/100}$ female mice (1/53) showed paraplegia and some (8/53) died suddenly but showed no macroscopically or microscopically noticeable findings that would explain the death. Nevertheless, ~16% LDLR$^{-/-}$ApoB$^{100/100}$ of control female mice displayed weakness to an extent that required the mice be euthanized or died suddenly (7/44) mainly at the age of 10-12 months, but did not show macroscopically or microscopically noticeable findings that would explain the death. The number of myocardial infarctions, sudden deaths, paraplegias and mice displaying coronary artery stenosis in Nrf2$^{-/-}$LDLR$^{-/-}$ApoB$^{100/100}$ and LDLR$^{-/-}$ApoB$^{100/100}$ female and male mice is shown in Table 3. We did not find any abdominal aortic aneurysms or other serious health problems in dissection or histopathological examination of female and male LDLR$^{-/-}$ApoB$^{100/100}$

and Nrf2$^{-/-}$LDLR$^{-/-}$ApoB$^{100/100}$ mice. We also analyzed coronary artery stenosis routinely at the age of 6 and 12 months and this analysis showed varied plaque sizes (data not shown).

We investigated cardiac function by Vevo® Ultrasound in LDLR$^{-/-}$ApoB$^{100/100}$ and Nrf2$^{-/-}$ LDLR$^{-/-}$ApoB$^{100/100}$ female mice at the age of 6 months but did not find any abnormalities, which could have predicted sudden deaths (Figure IVA-D in the online-only Data Supplement).

Nrf2 deficiency promotes plaque instability in aged LDLR$^{-/-}$ApoB$^{100/100}$ female mice

In mouse models of atherosclerosis, brachiocephalic artery typically shows a complex plaque morphology that mimics human like rupture-prone plaque morphology [37,38]. Thus, we analyzed the plaque phenotype more closely in brachiocephalic arteries and found that lesion morphology was very complex in both LDLR$^{-/-}$ApoB$^{100/100}$ and Nrf2$^{-/-}$LDLR$^{-/-}$ApoB$^{100/100}$ mice. Advanced fibrocalcific plaques with large lateral xanthomas were found, containing extracellular material, large necrotic cores with cholesterol crystals and only a few macrophages and smooth muscle cells, indicating a highly necrotic plaque landscape. Nrf2 deficiency did not have an effect on total plaque area (data not shown), but it reduced plaque area ~20% in relation to lumen area (data not shown) in brachiocephalic artery. Macrophage positive area (Figure 6A) in relation to plaque area was equal in both groups. Plaque necrotic area (Figure 6B) in relation to plaque area was not significantly different in Nrf2$^{-/-}$ LDLR$^{-/-}$ApoB$^{100/100}$ mice compared to LDLR$^{-/-}$ ApoB$^{100/100}$ mice. However, Nrf2 deficiency increased fibrofatty nodule area relative to lesion area by ~60% (Figure 6C) and lesion calcification normalized to lesion area by ~200% (Figure 6D) in LDLR$^{-/-}$ApoB$^{100/100}$ mice. Plaque collagen content (Figure 6E) was uniform in both groups, and plaque smooth muscle cell area relative to total lesion area was not significantly different in Nrf2$^{-/-}$ LDLR$^{-/-}$ApoB$^{100/100}$ in comparison to LDLR$^{-/-}$ApoB$^{100/100}$ mice detected by αSMA primary antibody (Figure 6F) or SMHC primary antibody (Figure IIC in the online-only Data Supplement). Plaque stability was defined as the thickness of fibrous cap that separates a necrotic core of an atherosclerotic plaque from the lumen. Interestingly, fibrous cap thickness was reduced by more than 30% in Nrf2-deficient LDLR$^{-/-}$ApoB$^{100/100}$ mice (Figure 6G) in comparison to LDLR$^{-/-}$ ApoB$^{100/100}$ mice. Moreover, plaque instability index[30,31,32] was calculated as a ratio between instability (macrophages, necrotic area) and stability (collagen, smooth muscle cells) factors and it was found that Nrf2 deficiency increased plaque instability index (Figure 6H) in LDLR$^{-/-}$ ApoB$^{100/100}$ mice. Also cap to core ratio (Figure 6I) was reduced in Nrf2-deficient LDLR$^{-/-}$ ApoB$^{100/100}$ mice in comparison to LDLR$^{-/-}$ApoB$^{100/100}$ mice.

Nrf2 deficiency promotes plaque inflammation and oxidative stress

Since persistent systemic and local plaque chronic inflammation predisposes to plaque maturation, we next examined MCP-1 and TNFα expression in brachiocephalic arteries and found that MCP-1 positive staining area (Figure 7A) was increased in Nrf2$^{-/-}$LDLR$^{-/-}$ApoB$^{100/100}$ mice compared to LDLR$^{-/-}$ApoB$^{100/100}$ mice at age of 12 months. TNFα positive staining area (Figure 7B) was not significantly different between the groups. We also measured the expression of key proinflammatory cytokines in bone marrow derived macrophages harvested from Nrf2$^{-/-}$LDLR$^{-/-}$ApoB$^{100/100}$ and LDLR$^{-/-}$ApoB$^{100/100}$ mice. In line with previous reports supporting anti-inflammatory actions of Nrf2[16,39], Nrf2 deficiency significantly increased gene expression of MCP-1 (Figure 7C), TNF-α (Figure 7D) IL-1β (Figure 7E) and IL-6 (Figure 7F) upon stimulation by LPS or AcLDL. Moreover, plasma pro-inflammatory cytokines MCP-1 and TNFα were measured (Figure 7H), but found not to be different between the study groups, likely because of high variation between the individual mice**.** In addition to inflammatory factors, we also measured plaque oxidative stress by staining the brachiocephalic sections with 4-HNE and 3-NT primary antibodies. Nrf2 deficiency increased 4-HNE positive staining (Figure 7I), but 3-NT staining (Figure 7J) was no different between the groups.

Discussion

Oxidative stress has been implicated in the initiation and progression of atherosclerosis from the early fatty streak lesions to the rupture and thrombosis of advanced atherosclerotic plaque[1]. Given that the redox-activated transcription factor Nrf2 is a ubiquitous factor affecting the gene expression of a vast number of genes mediating antioxidant protection and suppression of inflammation, it is logical to postulate that the loss of Nrf2 aggravates atherogenesis[16]. Nevertheless, several investigators have shown that the global loss of Nrf2 alleviates atherosclerosis in ApoE$^{-/-}$ hypercholesterolemic mice[19,20,21,18]. Due to the limitations of ApoE$^{-/-}$ mice to model human atherosclerosis, we used two alternative mouse models, LDLR$^{-/-}$ mice fed a high-fat diet as well as chow fed LDLR$^{-/-}$ApoB$^{100/100}$ mice that have a lipoprotein profile characteristic of human hypercholesteromia, to study the effect of global loss of Nrf2 on atherogenesis[36,22]. We discovered that Nrf2 deficiency decreased the extent of atherosclerosis measured by *en face* analysis as well as the size of atherosclerotic plaques in both mouse models. In a more human-like hypercholesterolemic LDLR$^{-/-}$ApoB$^{100/100}$ female mice, it also promoted plaque inflammation and oxidative stress that possibly led to an increased plaque instability, which is considered as a risk factor of MI and sudden death in humans.

While the previous reports have uniformly concluded that the global loss of Nrf2 results in the reduction of atherosclerotic lesion size in ApoE$^{-/-}$ mice, the postulated mechanisms vary from one study to another. The proposed mechanisms include decreased CD36 expression and hence reduced uptake of modified LDL[18,19], attenuated cholesterol crystal-induced inflammasome activation[20] as well as systemic effects via lowered plasma and liver cholesterol levels and reduced expression of lipogenic genes in the liver[19]. Given the differences in experimental design, it is hard to compare previous studies. For instance, two different Nrf2-deficient mouse strains were used, and the duration of diet, cholesterol content and age of euthanasia varied considerably[18,19,20]. Our study supports systemic metabolic effects of Nrf2 in high fat-fed LDLR$^{-/-}$Nrf2$^{-/-}$ mice. We show reduction in the size of atherosclerotic plaques, most likely because of decreased plasma cholesterol. The connection between Nrf2 and lipid biosynthesis has been observed, as two microarray analyses using gene modified mice indicated that Nrf2 regulates the expression of several genes involved in the regulation of fatty acid and cholesterol synthesis in the liver[40,41]. Additionally, in support of favorable metabolic effects, we found that Nrf2 deficiency reduced body weight of LDLR$^{-/-}$ mice on both regular chow and HFD. This is in line with previous studies, in which Nrf2 deficiency was protective against HFD induced weight gain via inhibition of adipogenesis due to impaired PPARγ signaling, and an increase in energy expenditure by increased UCP-1 expression in the liver and white adipose tissue[42,43]. It is known that murine models display sexual dimorphism in many hepatic genes involved in lipid metabolism and atherogenesis. This may well explain the differential effects in plasma lipids and atherosclerosis development between sexes in the present study[44].

Nrf2 has well known anti-inflammatory functions both *in vitro* as well as *in vivo* in mouse models of inflammation[45]. We and others have shown that Nrf2 and its target genes have local anti-atherogenic effects in the vascular wall, including endothelial cells and macrophages[16,12,39]. Hematopoietic cell-specific Nrf2 deficiency aggravates inflammation and accelerates atherogenesis in both early[16] and late[17] stages of atherosclerosis. Recent findings indicate that Nrf2 directly represses inflammatory gene expression in macrophages via binding to the proximity of select proinflammatory genes such as cytokines, thereby inhibiting RNA Polymerase II binding and gene transcription[39]. In this study, Nrf2$^{-/-}$LDLR$^{-/-}$ mice that represent earlier stages of atherosclerosis (resembling fatty streak and uncomplicated lesions, type I-II)[35] had a higher amount of macrophages normalized to the lesion area, whereas in Nrf2$^{-/-}$LDLR$^{-/-}$ApoB$^{100/100}$ mice the plaques were far more mature, containing significantly enlarged necrotic and acellular areas and increased calcification and thinned fibrous caps. These results suggest that Nrf2 deficiency delays atherogenesis in both models, but has different effects on plaque

morphology depending on the plaque type. Moreover, expression of MCP-1 was significantly increased in the atherosclerotic plaques of $Nrf2^{-/-}LDLR^{-/-}ApoB^{100/100}$ mice in comparison to $LDLR^{-/-}ApoB^{100/100}$ mice indicating increased local plaque inflammation. MCP-1 plays a role plaque instability by regulating matrix metalloproteinase (MMP) expression, and it has been reported that an inhibitory antibody to MCP-1 in $ApoE^{-/-}$ mice increased plaque stability by increasing plaque collagen content[46,47,48]. As plaque macrophages have an important role in plaque stability, we also studied bone marrow derived macrophages derived from $Nrf2^{-/-}LDLR^{-/-}ApoB^{100/100}$ mice and found that they were more inflammatory, showing increased mRNA expression of key proinflammatory cytokines upon proinflammatory stimuli. Given that defective resolution of inflammation plays a central role in the progression of an atheroma to a rupture-prone advanced lesion and that Nrf2 is the key transmitter of the actions of pro-resolving lipid mediators,[49,50]. It is likely that persistent inflammation within the lesions leads to an unstable plaque phenotype and increases the risk of MI seen in Nrf2-deficient $LDLR^{-/-}ApoB^{100/100}$ mice.

In summary, our results demonstrate that whole body Nrf2 deficiency delays atherogenesis measured by the size of atherosclerotic plaques but that it also promotes plaque instability in later stages of the disease. This study highlights differences between mouse models of atherosclerosis and the need for a variety of models to tease out phenotypic differences. Given that Nrf2 activators are under active drug development or already in clinical use (dimethyl fumarate, Tecfidera® for multiple sclerosis), it is of utmost importance to clarify the role of Nrf2 in cardiometabolic diseases. This is especially relevant as these drugs are intended for long term use also in younger subjects and therefore any adverse health effects should be closely monitored. At this juncture, it is important to note that the Bardoxolone Methyl Evaluation in Patients with Chronic Kidney Disease and Type 2 Diabetes (BEACON), trial was prematurely terminated after preliminary analyses showed that patients randomized to bardoxolone methyl experienced significantly higher rates of heart failure events. However, it was suggested that these effects we mediated by the interference with the endothelin system[52]. There is no data suggesting that Nrf2 activators would aggravate atherogenesis in humans, but longer follow-up times are necessary to draw any definite conclusions. Moreover, further studies utilizing tissue-specific gene modified mice are warranted in order to define the contribution of Nrf2 in different tissues and cell types on the atherogenic process.

Sources of funding

This study was funded by the Academy of Finland, the Sigrid Juselius Foundation, the Finnish Cultural Foundation, the Saara Kuusisto Foundation and the Foundation of Cardiovascular Research in Finland.

Acknowledgements

Arja Korhonen, Anne Seppänen, Seija Sahrio, Jari Metso, Sari Nuutinen and Kuopio Biomedical Imaging Unit are acknowledged for their technical assistance. Nihay Laham Karam is acknowledged for the proofreading the manuscript. We thank the personnel of the Laboratory Animal Center, especially Auli Nissinen and Eveliina Kyllönen for the animal care.

Conflict of interest

None.

References

1. Christopher Glass AK, Witztum JL. Atherosclerosis: The Road Ahead Review approach to evaluating potential roles of specific pro. *Cell*. 2001;104:503–516.

2. Ylä-Herttuala S, Bentzon JF, Daemen M, Falk E, Garcia-Garcia HM, Herrmann J, Hoefer I, Jauhiainen S, Jukema JW, Krams R, Kwak BR, Marx N, Naruszewicz M, Newby A, Pasterkamp G, Serruys PWJC, Waltenberger J, Weber C, Tokgozoglu L. Stabilization of atherosclerotic plaques: An update. *Eur Heart J*. 2013;34:3251–3258.

3. Bentzon JF, Otsuka F, Virmani R, Falk E. Mechanisms of plaque formation and rupture. *Circ Res*. 2014;114:1852–1866.

4. Sugamura K, Keaney JF. Reactive oxygen species in cardiovascular disease. Free Radic. Biol. Med. 2011;51:978–992.

5. Libby P, Ridker PM, Maseri A. Inflammation and atherosclerosis. *Circulation*. 2002;105:1135–1143.

6. Yia-Herttuala S, Palinski W, Rosenfeld ME, Parthasarathy S, Carew TE, Butler S, Witztum JL, Steinberg D. Evidence for the presence of oxidatively modified low density lipoprotein in atherosclerotic lesions of rabbit and man. *J Clin Invest*. 1989;84:1086–1095.

7. Kisucka J, Chauhan AK, Patten IS, Yesilaltay A, Neumann C, Van Etten RA, Krieger M, Wagner DD. Peroxiredoxin1 prevents excessive endothelial activation and early atherosclerosis. *Circ Res*. 2008;103:598–605.

8. Orozco LD, Kapturczak MH, Barajas B, Wang X, Weinstein MM, Wong J, Deshane J, Bolisetty S, Shaposhnik Z, Shih DM, Agarwal A, Lusis AJ, Araujo JA. Heme oxygenase-1 expression in macrophages plays a beneficial role in atherosclerosis. *Circ Res*. 2007;100:1703–1711.

9. Park JG, Yoo JY, Jeong SJ, Choi JH, Lee MR, Lee MN, Hwa Lee J, Kim HC, Jo H, Yu DY, Kang SW, Rhee SG, Lee MH, Oh GT. Peroxiredoxin 2 deficiency exacerbates atherosclerosis in apolipoprotein E-deficient mice. *Circ Res*. 2011;109:739–749.

10. Cheng C, Noordeloos AM, Jeney V, Soares MP, Moll F, Pasterkamp G, Serruys PW, Duckers HJ. Heme oxygenase 1 determines atherosclerotic lesion progression into a vulnerable plaque. *Circulation*. 2009;119:3017–3027.

11. Ruotsalainen A-K, Inkala M, Partanen ME, Lappalainen JP, Kansanen E, Mäkinen PI, Heinonen SE, Laitinen HM, Heikkilä J, Vatanen T, Hörkkö S, Yamamoto M, Ylä-Herttuala S, Jauhiainen M, Levonen A-L. The absence of macrophage Nrf2 promotes early atherogenesis. *Cardiovasc Res*. 2013;98:107–15.

12. Jyrkkänen H-K, Kansanen E, Inkala M, Kivelä AM, Hurttila H, Heinonen SE, Goldsteins G, Jauhiainen S, Tiainen S, Makkonen H, Oskolkova O, Afonyushkin T, Koistinaho J, Yamamoto M, Bochkov VN, Ylä-Herttuala S, Levonen A-L. Nrf2 regulates antioxidant gene expression evoked by oxidized phospholipids in endothelial cells and murine arteries in vivo. *Circ Res*. 2008;103:e1–9.

13. Hosoya T, Maruyama A, Kang M Il, Kawatani Y, Shibata T, Uchida K, Itoh K, Yamamoto M. Differential responses of the Nrf2-Keap1 system to laminar and oscillatory shear

stresses in endothelial cells. *J Biol Chem*. 2005;280:27244–27250.

14. Zakkar M, Heiden K Van Der, Luong LA, Chaudhury H, Cuhlmann S, Hamdulay SS, Krams R, Edirisinghe I, Rahman I, Carlsen H, Haskard DO, Mason JC, Evans PC. Activation of Nrf2 in Endothelial Cells Protects Arteries From Exhibiting a Proinflammatory State. 2009;

15. Levonen AL, Inkala M, Heikura T, Jauhiainen S, Jyrkkänen HK, Kansanen E, Määttä K, Romppanen E, Turunen P, Rutanen J, Ylä-Herttuala S. Nrf2 gene transfer induces antioxidant enzymes and suppresses smooth muscle cell growth in vitro and reduces oxidative stress in rabbit aorta in vivo. *Arterioscler Thromb Vasc Biol*. 2007;27:741–747.

16. Ruotsalainen AK, Inkala M, Partanen ME, Lappalainen JP, Kansanen E, Mäkinen PI, Heinonen SE, Laitinen HM, Heikkilä J, Vatanen T, Hörkkö S, Yamamoto M, Ylä-Herttuala S, Jauhiainen M, Levonen AL. The absence of macrophage Nrf2 promotes early atherogenesis. *Cardiovasc Res*. 2013;98:107–115.

17. Collins AR, Gupte AA, Ji R, Ramirez MR, Minze LJ, Liu JZ, Arredondo M, Ren Y, Deng T, Wang J, Lyon CJ, Hsueh WA. Myeloid deletion of nuclear factor erythroid 2-related factor 2 increases atherosclerosis and liver injury. *Arterioscler Thromb Vasc Biol*. 2012;32:2839–2846.

18. Sussan TE, Jun J, Thimmulappa R, Bedja D, Antero M, Gabrielson KL, Polotsky VY, Biswal S. Disruption of Nrf2, a key inducer of antioxidant defenses, attenuates ApoE-mediated atherosclerosis in mice. *PLoS One*. 2008;3.

19. Barajas B, Che N, Yin F, Rowshanrad A, Orozco LD, Gong KW, Wang X, Castellani LW, Reue K, Lusis AJ, Araujo JA. NF-E2-related factor 2 promotes atherosclerosis by effects on plasma lipoproteins and cholesterol transport that overshadow antioxidant protection. *Arterioscler Thromb Vasc Biol*. 2011;31:58–66.

20. Freigang S, Ampenberger F, Spohn G, Heer S, Shamshiev AT, Kisielow J, Hersberger M, Yamamoto M, Bachmann MF, Kopf M. Nrf2 is essential for cholesterol crystal-induced inflammasome activation and exacerbation of atherosclerosis. *Eur J Immunol*. 2011;41:2040–2051.

21. Harada N, Ito K, Hosoya T, Mimura J, Maruyama A, Noguchi N, Yagami KI, Morito N, Takahashi S, Maher JM, Yamamoto M, Itoh K. Nrf2 in bone marrow-derived cells positively contributes to the advanced stage of atherosclerotic plaque formation. *Free Radic Biol Med*. 2012;53:2256–2262.

22. Curtiss LK, Boisvert W a. Apolipoprotein E and atherosclerosis. *Curr Opin Lipidol*. 2000;11:243–251.

23. Ishibashi S, Herz J, Maeda N, Goldstein JL, Brown MS. The two-receptor model of lipoprotein clearance: tests of the hypothesis in “knockout” mice lacking the low density lipoprotein receptor, apolipoprotein E, or both proteins. *Proc Natl Acad Sci U S A*. 1994;91:4431–5.

24. Langer C, Huang Y, Cullen P, Wiesenhütter B, Mahley RW, Assmann G, von Eckardstein A. Endogenous apolipoprotein E modulates cholesterol efflux and cholesteryl ester hydrolysis mediated by high-density lipoprotein-3 and lipid-free apolipoproteins in mouse peritoneal macrophages. *J Mol Med (Berl)*. 2000;78:217–227.

25. Zanotti I, Pedrelli M, Potì F, Stomeo G, Gomaraschi M, Calabresi L, Bernini F. Macrophage, but not systemic, apolipoprotein e is necessary for macrophage reverse cholesterol transport in vivo. *Arterioscler Thromb Vasc Biol*. 2011;31:74–80.

26. Véniant MM, Zlot CH, Walzem RL, Pierotti V, Driscoll R, Dichek D, Herz J, Young SG. Lipoprotein clearance mechanisms in LDL receptor-deficient “apo-B48- only” and “apo-B100-only” mice. *J Clin Invest*. 1998;102:1559–1568.

27. Véniant MM, Withycombe S, Young SG. Lipoprotein size and atherosclerosis susceptibility in Apoe(-/-) and Ldlr(-/-) mice. *Arterioscler Thromb Vasc Biol*. 2001;21:1567–70.

28. Veniant MM, Beigneux AP, Bensadoun A, Fong LG, Young SG. Lipoprotein size and susceptibility to atherosclerosis - Insights from genetically modified mouse models. *Curr Drug Targets*. 2008;9:174.

29. Getz GS, Reardon CA. Diet and murine atherosclerosis. *Arterioscler Thromb Vasc Biol*. 2006;26:242–249.

30. Dong M, Yang X, Lim S, Cao Z, Honek J, Lu H, Seki T, Hosaka K, Wahlberg E, Yang J, Zhang L, Dong M, Yang X, Lim S, Cao Z, Honek J, Lu H, Seki T, Hosaka K, Wahlberg E, Yang J, Zhang L, Lipolysis U. Cold Exposure Promotes Atherosclerotic Plaque Growth and Instability via UCP1- Dependent Lipolysis Short Article Cold Exposure Promotes Atherosclerotic Plaque Growth and Instability. 2013.

31. Hartwig H, Silvestre-roig C, Hendrikse J, Beckers L. Atherosclerotic Plaque Destabilization in Mice : A Comparative Study. 2015;1–14.

32. Shiomi M, Ito T, Hirouchi Y, Enomoto M. Fibromuscular cap composition is important for the stability of established atherosclerotic plaques in mature WHHL rabbits treated with statins. 2001;157:75–84.

33. Thomas EL, Modi N, Frost G, Coutts GA, Bell JD. Fast and Reproducible Method for the Direct Quantitation of Adipose Tissue in. 2002;37.

34. Merentie M, Lottonen-Raikaslehto L, Parviainen V, Huusko J, Pikkarainen S, Mendel M, Laham-Karam N, Karja V, Hedman M, Yla-Herttuala S. Efficacy and safety of myocardial gene transfer of adenovirus, adeno-associated virus and lentivirus vectors in mouse heart. *Gene Ther*. 2015;1–10.

35. Virmani R, Virmani R, Kolodgie FD, Kolodgie FD, Burke AP, Burke AP, Farb A, Farb A, Schwartz SM, Schwartz SM. Lessons From Sudden Coronary Death. *Arterioscler Thromb*. 2000;1262–1275.

36. Farese R V, Véniant MM, Cham CM, Flynn LM, Pierotti V, Loring JF, Traber M, Ruland S, Stokowski RS, Huszar D, Young SG. Phenotypic analysis of mice expressing exclusively apolipoprotein B48 or apolipoprotein B100. *Proc Natl Acad Sci U S A*. 1996;93:6393–6398.

37. Jackson CL, Bond AR. The fat-fed apolipoprotein e knockout mouse brachiocephalic artery in the study of atherosclerotic plaque rupture. *J Biomed Biotechnol*. 2011.

38. Rosenfeld ME, Polinsky P, Virmani R, Kauser K, Rubanyi G, Schwartz SM. Advanced atherosclerotic lesions in the innominate artery of the ApoE knockout mouse. *Arterioscler*

Thromb Vasc Biol. 2000;20:2587–2592.

39. Kobayashi EH, Suzuki T, Funayama R, Nagashima T, Hayashi M, Sekine H, Tanaka N, Moriguchi T, Motohashi H, Nakayama K, Yamamoto M. Nrf2 suppresses macrophage inflammatory response by blocking proinflammatory cytokine transcription. *Nat Commun*. 2016;7:11624.

40. Kitteringham NR, Abdullah A, Walsh J, Randle L, Jenkins RE, Sison R, Goldring CEP, Powell H, Sanderson C, Williams S, Higgins L, Yamamoto M, Hayes J, Park BK. Proteomic analysis of Nrf2 deficient transgenic mice reveals cellular defence and lipid metabolism as primary Nrf2-dependent pathways in the liver. *J Proteomics*. 2010;73:1612–1631.

41. Chartoumpekis D V, Ziros PG, Zaravinos A, Iskrenova RP, Psyrogiannis AI, Kyriazopoulou VE, Sykiotis GP, Habeos IG. Hepatic Gene Expression Profiling in Nrf2 Knockout Mice after Long-Term High-Fat Diet-Induced Obesity. 2013;2013.

42. Pi J, Leung L, Xue P, Wang W, Hou Y, Liu D, Yehuda-Shnaidman E, Lee C, Lau J, Kurtz TW, Chan JY. Deficiency in the nuclear factor E2-related factor-2 transcription factor results in impaired adipogenesis and protects against diet-induced obesity. *J Biol Chem*. 2010;285:9292–9300.

43. Schneider K, Valdez J, Nguyen J, Vawter M, Galke B, Kurtz TW, Chan JY. Increased energy expenditure, ucp1 expression, and resistance to diet-induced obesity in mice lacking nuclear factor-erythroid-2-related transcription factor-2 (nrf2). *J Biol Chem*. 2016;291:7754–7766.

44. Yang X, Schadt EE, Wang S, Wang H, Arnold AP, Ingram-Drake L, Drake TA, Lusis AJ. Tissue-specific expression and regulation of sexually dimorphic genes in mice. *Genome Res*. 2006;16:995–1004.

45. Thimmulappa RK, Lee H, Rangasamy T, Reddy SP, Yamamoto M, Kensler TW, Biswal S. Nrf2 is a critical regulator of the innate immune response and survival during experimental sepsis. *J Clin Invest*. 2006;116:984–995.

46. Lutgens E, Faber B, Schapira K, Evelo CTA, Haaften R Van, Heeneman S, Cleutjens KBJM, Bijnens AP, Beckers L, Porter JG, Mackay CR, Rennert P, Bailly V, Jarpe M, Dolinski B, Koteliansky V, Fougerolles T De, Daemen MJAP. Gene Profiling in Atherosclerosis Reveals a Key Role for Validation Using a Novel Monocyte Chemoattractant Protein Monoclonal Antibody. 2005;

47. Inoue S, Egashira K, Ni W, Kitamoto S, Usui M. Basic Science Reports Limits Progression and Destabilization of Established Atherosclerosis in Apolipoprotein E – Knockout Mice. 2002;2700–2707.

48. Fuchs S.a, d · Lavi I.e · Tzang O.e · Bessler H.b, d · Brosh D.c · Bental T.c · Dvir D.c · Einav S.e · Kornowski R.c d. Intracoronary monocyte chemoattractant protein 1 and vascular endothelial growth factor levels are associated with necrotic core, calcium and fibrous tissue atherosclerotic plaque components: an intracoronary ultrasound radiofrequency study. *Cardiology*. 2012;123:125–132.

49. Bretscher P, Egger J, Shamshiev A, Trötzmüller M, Köfeler H, Carreira EM, Kopf M, Freigang S, Peter Bretscher, Julian Egger, Abdijapar Shamshiev, Martin Trötzmüller HK,

Erick M Carreira, Manfred Kopf & SF, Bretscher P, Egger J, Shamshiev A, Trötzmüller M, Köfeler H, Carreira EM, Kopf M, Freigang S. Phospholipid oxidation generates potent anti-inflammatory lipid mediators that mimic structurally related pro-resolving eicosanoids by activating Nrf 2. *EMBO Mol Med*. 2015;7:1–16.

50. Groeger AL, Cipollina C, Cole MP, Woodcock SR, Bonacci G, Rudolph TK, Rudolph V, Freeman BA, Schopfer FJ. Cyclooxygenase-2 generates anti-inflammatory mediators from omega-3 fatty acids. *Nat Chem Biol*. 2010;6:433–41.

51. Pineda A, Sierra S, Tercero I, Va JA, Burgos JS. ApoB100 / LDLR- / - Hypercholesterolaemic Mice as a Model for Mild Cognitive Impairment and Neuronal Damage. 2011;6.

52. Chin MP, Reisman A, Bakris GL, Grady O. Mechanisms Contributing to Adverse Cardiovascular Events in Patients with Type 2 Diabetes Mellitus and Stage 4 Chronic Kidney Disease Treated with Bardoxolone Methyl. 2014;75063:499–508.

Table 1. Characteristics of Nrf2$^{-/-}$LDLR$^{-/-}$ and LDLR$^{-/-}$ male and female mice on a high-fat-diet.

Strain		**LDLR$^{-/-}$** Male n=12 Female n=10	**Nrf2$^{-/-}$LDLR$^{-/-}$** Male n=9 Female n=7	**LDLR$^{-/-}$** Male n=14 Female n=4	**Nrf2$^{-/-}$LDLR$^{-/-}$** Male n=13 Female n=8	**LDLR$^{-/-}$** Male n=8 Female n=16	**Nrf2$^{-/-}$LDLR$^{-/-}$** Male n=9 Female n=7
point (wk)	**Gender**	**0**		**6**		**12**	
Body weight (g)	Male	29.8±3.4	26.0±3.5*****	37.6±4.0	33.5±5.4*****	43.1±6.9	36.8±4.6
	Female	19.3±0.8	17.8±1.5*****	23.2±2.1	22.0±3.9	23.5±3.2	21.9±1.1
Total cholesterol (mmol/l)	Male	5.6±1.5	4.7±1.2	29.3±5.9	25.6±7.8*****	32.7±3.2	34.3±6.0
	Female	3.5±1.4	3.9±1.7	26.0±4.8	18.9±4.2	23.3±3.4	26.0±8.9
Triglycerides (mmol/l)	Male	1.5±0.7	1.3±0.4	2.7±1.8	2.2±0.9	4.0±1.7	7.5±2.7*****
	Female	2.3±1.1	1.4±1.3	1.7±0.9	1.8±0.9	1.7±0.4	1.9±1.1

Data are expressed as mean ± SD. * $p< 0.05$ Nrf2$^{-/-}$LDLR $^{-/-}$ versus LDLR$^{-/-}$.

Table 2. Characteristics of Nrf2$^{-/-}$LDLR$^{-/-}$ApoB$^{100/100}$ and LDLR$^{-/-}$ApoB$^{100/100}$ male and female mice on a regular chow diet.

Strain		**LDLR$^{-/-}$ApoB$^{100/100}$**		**Nrf2$^{-/-}$LDLR$^{-/-}$ ApoB$^{100/100}$**	
Time point (months)	**Gender**	**6** Male n=12 Female n=7	**12** Male n=9 Female n=22	**6** Male n=7 Female n=10	**12** Male n=13 Female n=12
Body weight (g)	Male	33.3±3.0	37.2±2.5	35.0±3.2	31.9±1.7*
	Female	24.1±3.0	32.4±2.1	21.5±1.4*	27.5±6.3
Total cholesterol (mmol/l)	Male	7.6±3.0	14.1±5.0	6.7±1.9	6.5±3.8*
	Female	7.5±3.0	8.1±2.8	6.5±2.4	8.2±2.7
Triglycerides (mmol/l)	Male	1.9±0.4	2.3±1.1	1.7±0.6	1.7±0.9
	Female	1.8±0.3	1.4±0.4	1.2±0.3*	1.1±0.4*

Data are expressed as mean ± SD. * p< 0.05 Nrf2$^{-/-}$LDLR $^{-/-}$ApoB$^{100/100}$ versus LDLR$^{-/-}$ApoB$^{100/100}$.

Table 3. Incidence of myocardial infarctions, sudden deaths, paraplegias and coronary artery stenosis during aging in $Nrf2^{-/-}LDLR^{-/-}ApoB^{100/100}$ and $LDLR^{-/-}ApoB^{100/100}$ male and female mice.

Strain		$LDLR^{-/-}ApoB^{100/100}$	$Nrf2^{-/-}LDLR^{-/-}$ $ApoB^{100/100}$
Myocardial infarction	Male	0/30	0/15
	Female	0/44	10/53*
Sudden death	Male	0/30	3/15
	Female	7/44	8/53
Paraplegia	Male	1/30	1/15
	Female	1/44	1/53
Deaths in total	Male	1/30	4/15*
	Female	8/44	19/53*
Coronary artery stenosis	Male	8/14	5/13
	Female	18/20	9/14

* $p < 0.05$ $Nrf2^{-/-}LDLR^{-/-}ApoB^{100/100}$ versus $LDLR^{-/-}ApoB^{100/100}$

Figure Legends

Figure 1. Nrf2 deficiency impairs development of diet-induced atherosclerosis in LDLR$^{-/-}$ male mice. LDLR$^{-/-}$ (white dots) and Nrf2$^{-/-}$LDLR$^{-/-}$ (red dots) male mice were fed HFD for 6 or 12 wk. **A,** Quantification of cross-sectional lesion area (μm^2) from aortic root of LDLR$^{-/-}$ and Nrf2$^{-/-}$ LDLR$^{-/-}$ mice. Representative pictures of hematoxylin-eosin stained sections. **B**, Lesion coverage of entire aorta (%) by *en face* analysis with representative pictures of Oil Red O stained aortas. Representative pictures of aortic root are shown with a scale bar 100 μm and en face aortas with a scale bar 1 mm. Each dot represents one mouse and the horizontal line represents mean ± SEM, statistical significance *P<0.05, **P<0.01 by Student's *t*-test. Number of mice analyzed: 6 wk HFD LDLR$^{-/-}$ n=7 and Nrf2$^{-/-}$LDLR$^{-/-}$ n=3-8, 12 weeks HFD LDLR$^{-/-}$ n=7-10 and Nrf2$^{-/-}$LDLR$^{-/-}$ n=15-10.

Figure 2. Nrf2 deficiency increases macrophage positive area in aortic plaques of LDLR$^{-/-}$ male mice. LDLR$^{-/-}$ (white dots) and Nrf2$^{-/-}$LDLR$^{-/-}$ mice (red dots) were fed HFD for 6 or 12 wk. **A,** Macrophage positive lesion area normalized to total lesion area (%) and measured from the aortic root. Representative pictures of mMQ immunostained sections (macrophage positive area is outlined with a dotted line). **B**, Lesion necrotic area (%) normalized to total lesion area from hematoxylin-eosin stained aortic root sections after 12 wk HFD (necrotic area outlined with a dotted line). Representative pictures are shown with a scale bar 100 μm. Each dot represents one mouse and the horizontal line represents mean ± SEM, *P<0.05, ***P<0.001 by Student's *t*-test. Number of mice analyzed: 6 wk HFD LDLR$^{-/-}$ n=11 and Nrf2$^{-/-}$LDLR$^{-/-}$ n=11, 12 weeks HFD LDLR$^{-/-}$ n=7 and Nrf2$^{-/-}$LDLR$^{-/-}$ n=6-10.

Figure 3. **Nrf2 deficiency impairs development of ageing-induced atherosclerosis in LDLR$^{-/-}$ApoB$^{100/100}$ female mice.** LDLR$^{-/-}$ApoB$^{100/100}$ (white dots) and Nrf2$^{-/-}$LDLR$^{-/-}$ApoB$^{100/100}$ female mice (red dots) were aged for 6 or 12 months on a chow diet. **A,** Quantification of cross-sectional lesion area (μm^2) from aortic root of LDLR$^{-/-}$ApoB$^{100/100}$ and Nrf2$^{-/-}$LDLR$^{-/-}$ApoB$^{100/100}$ female mice at the age of 6 or 12 months. Representative pictures of hematoxylin-eosin stained sections. **B,** Lesion coverage of descending aorta (%) by *en face* analysis of 12-month-old female mice. Representative pictures of aortic root are shown with a scale bar 100 μm and en face aortas with a scale bar of 1 mm. Each dot represents one mouse and the horizontal line represents mean ± SEM, *P<0.05 by Student's *t*-test. Number of mice analyzed: 6-month-old LDLR$^{-/-}$ApoB$^{100/100}$ n=14 and Nrf2$^{-/-}$LDLR$^{-/-}$ApoB$^{100/100}$ n=13, 12-month-old LDLR$^{-/-}$ApoB$^{100/100}$ n=10-12 and Nrf2$^{-/-}$LDLR$^{-/-}$ApoB$^{100/100}$ n=8.

Figure 4. **Nrf2 deficiency promotes necrosis and calcification in fibroatheroma plaques in LDLR$^{-/-}$ApoB$^{100/100}$ female mice.** LDLR$^{-/-}$ApoB$^{100/100}$ (white dots) and Nrf2$^{-/-}$LDLR$^{-/-}$ApoB$^{100/100}$ female mice (red dots) were aged for 6 or 12 months on a chow diet. **A,** Lesion macrophage positive lesion area (outlined with a dotted line), **B**, necrotic area (hematoxylin-eosin staining, necrotic area outlined with a dotted line) **C**, plaque calcification (Alizarin Red S staining, black arrows depict red-stained calcifications) and **D**, 4-HNE positive lesion area measured in relation to total lesion area (%) in aortic root sections. Representative pictures are shown with a scale

bar 100 μm. Each dot represents one mouse and the horizontal line represents mean ± SEM, *P<0.05, **P<0.01 by Student's *t*-test. Number of mice analyzed: 6-month-old $LDLR^{-/-}ApoB^{100/100}$ n=7-13 and $Nrf2^{-/-}LDLR^{-/-}ApoB^{100/100}$ n=6-12, 12-month-old $LDLR^{-/-}ApoB^{100/100}$ n=7-11 and $Nrf2^{-/-}LDLR^{-/-}ApoB^{100/100}$ n=6-7.

Figure 5. Nrf2 deficiency predisposes to myocardial infarction and sudden death in $LDLR^{-/-}ApoB^{100/100}$ female mice. A, Survival curve (%) of $LDLR^{-/-}ApoB^{100/100}$ (n=53) and $Nrf2^{-/-}LDLR^{-/-}ApoB^{100/100}$ (n=44) female and $LDLR^{-/-}ApoB^{100/100}$ (n=30) and $Nrf2^{-/-}LDLR^{-/-}ApoB^{100/100}$ (n=15) male mice until the age of 12 months, when mice were sacrificed for analysis. **B**, Representative pictures of hematoxylin-eosin stained coronary artery sections from $Nrf2^{-/-}LDLR^{-/-}ApoB^{100/100}$ female mice died of myocardial infarction at the age of 7 months. Coronary arteries are indicated by black arrows and aortic lumen by black star. **C**, Myocardium sections of $Nrf2^{-/-}LDLR^{-/-}ApoB^{100/100}$ female mice were stained with Masson Trichrome. Histopathological examination revealed regional fibrotic scar tissue formation (indicated by black arrows) in infarcted area. Representative pictures are shown with a scale bar 100 μm, statistical significance *P<0.05, **P<0.01 by Log-rank test.

Figure 6. Nrf2 deficiency promotes plaque instability in brachiocephalic artery of aged $LDLR^{-/-}ApoB^{100/100}$ female mice. $LDLR^{-/-}ApoB^{100/100}$ (n=8-10) (white dots) and $Nrf2^{-/-}LDLR^{-/-}ApoB^{100/100}$ mice (n=6-9) (red dots) were sacrificed at the age of 12 months and plaque compositions was analysed from the brachiocephalic artery. Characteristics of instabile plaque, such as **A**, macrophage area stained with representative pictures of mMQ stained sections, **B**, necrotic core area analysed from Masson Trichrome stained sections and **C**, fibrofatty nodule area (outlined with a dotted line) was analysed from Movat´s Pentachrome staining and all the quantifications were normalized to total lesion area, with representative pictures. **D**, Plaque calcification (%) was analysed from Alizarin Red S stained sections (black arrows depicit red-stained calcification) in relation to total lesion area with representative pictures. Characteristics of stabile plaque, such as **E**, plaque collagen content was evaluated from Picro Sirius Red staining and **F**, smooth muscle cell content from αSMA stained sections in relation to plaque area with representative pictures. **G**, The fibrous cap thickness (μm), was measured from Masson´s Trichrome stained sections, with representative pictures from thinned cap (indicated by black arrows). **H**, Plaque instability index and **I**, cap to core ratio were calculated as based on plaque morphological analysis, described more in detail in methods. Representative pictures are shown with a scale bar 100 μm. Each dot represents one mouse and the horizontal line represents mean±SEM. *P<0.05, * P<0.05, **P<0.01, ***P<0.001 by Student's *t*-test.

Figure 7. Nrf2 deficiency promotes inflammation and oxidative stress in atheroma plaque. $LDLR^{-/-}ApoB^{100/100}$ (n=6-9) (white dots) and $Nrf2^{-/-}LDLR^{-/-}ApoB^{100/100}$ mice (n=5-6) (red dots) were sacrificed at the age of 12 months and plaque inflammation was analysed from the brachiocephalic artery. Quantification of **A**, MCP-1 positive staining area (indicated by black arrows) in relation to plaque area with representative pictures, and **B**, TNFα positive staining area in relation to plaque area. $LDLR^{-/-}ApoB^{100/100}$ and $Nrf2^{-/-}LDLR^{-/-}ApoB^{100/100}$ bone marrow cells were isolated and differentiated to macrophages. mRNA expression of pro-inflammatory

cytokines **C**, MCP-1, **D**, TNF-α, **E**, IL-1β and **F**, IL-6 were detected in basal conditions (n=4) and after treatment with AcLDL (n=6) or LPS (n=6) in bone marrow derived macrophages. Plasma **G**, MCP-1 and **H**, TNFα levels were measured from $LDLR^{-/-}ApoB^{100/100}$ (n=4) and $Nrf2^{-/-}LDLR^{-/-}ApoB^{100/100}$ mice (n=5). Plaque **I**, 4-HNE and **J**, 3-NT positive plaque area (%) (indicated by black arrows) normalized to total plaque area with representative sections. Representative pictures are shown with a scale bar 100 μm. Each dot represents one mouse and the horizontal line represents mean ± SEM, *P<0.05, **P<0.01, ***P<0.001 by Student's *t*-test.

Figure 1

FIG 1.

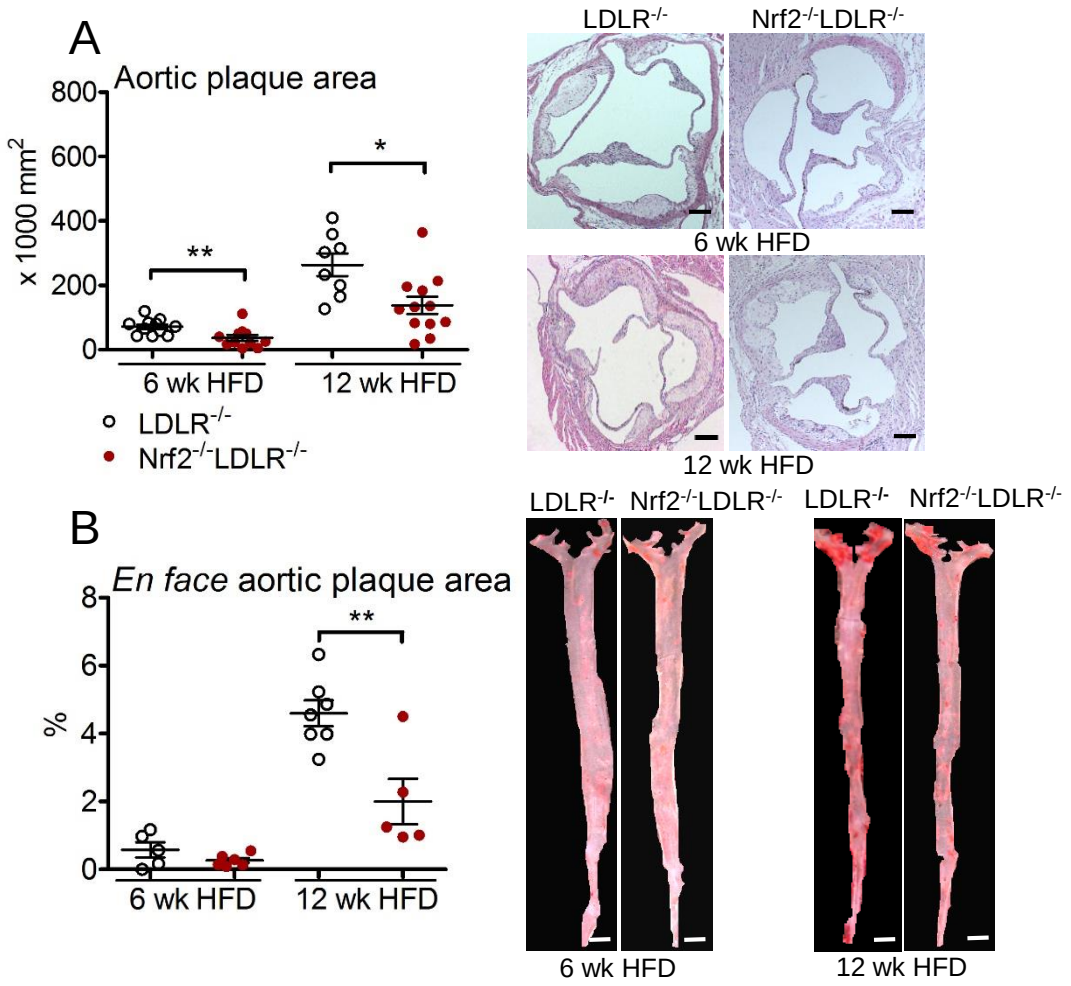

Figure 1. Nrf2 deficiency impairs development of diet-induced atherosclerosis in LDLR$^{-/-}$ male mice. LDLR$^{-/-}$ (white dots) and Nrf2$^{-/-}$LDLR$^{-/-}$ (red dots) male mice were fed HFD for 6 or 12 wk. **A,** Quantification of cross-sectional lesion area (μm^2) from aortic root of LDLR$^{-/-}$ and Nrf2$^{-/-}$LDLR$^{-/-}$ mice. Representative pictures of hematoxylin-eosin stained sections. **B**, Lesion coverage of entire aorta (%) by *en face* analysis with representative pictures of Oil Red O stained aortas. Representative pictures of aortic root are shown with a scale bar 100 μm and en face aortas with a scale bar 1 mm. Each dot represents one mouse and the horizontal line represents mean ± SEM, statistical significance *P<0.05, **P<0.01 by Student's *t*-test. Number of mice analyzed: 6 wk HFD LDLR$^{-/-}$ n=7 and Nrf2$^{-/-}$LDLR$^{-/-}$ n=3-8, 12 weeks HFD LDLR$^{-/-}$ n=7-10 and Nrf2$^{-/-}$LDLR$^{-/-}$ n=15-10.

Figure 2

FIG 2.

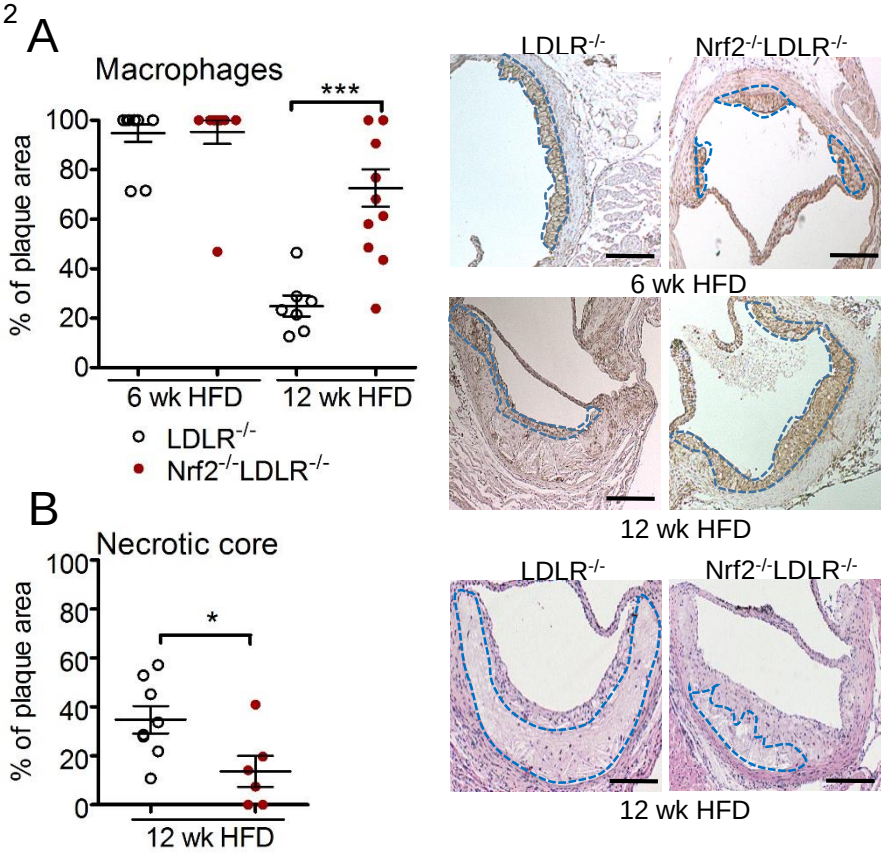

Figure 2. Nrf2 deficiency increases macrophage positive area in aortic plaques of LDLR$^{-/-}$ male mice. LDLR$^{-/-}$ (white dots) and Nrf2$^{-/-}$LDLR$^{-/-}$ mice (red dots) were fed HFD for 6 or 12 wk. **A,** Macrophage positive lesion area normalized to total lesion area (%) and measured from the aortic root. Representative pictures of mMQ immunostained sections (macrophage positive area is outlined with a dotted line). **B**, Lesion necrotic area (%) normalized to total lesion area from hematoxylin-eosin stained aortic root sections after 12 wk HFD (necrotic area outlined with a dotted line). Representative pictures are shown with a scale bar 100 µm. Each dot represents one mouse and the horizontal line represents mean ± SEM, *P<0.05, ***P<0.001 by Student's *t*-test. Number of mice analyzed: 6 wk HFD LDLR$^{-/-}$ n=11 and Nrf2$^{-/-}$LDLR$^{-/-}$ n=11, 12 weeks HFD LDLR$^{-/-}$ n=7 and Nrf2$^{-/-}$LDLR$^{-/-}$ n=6-10.

Figure 3

FIG 3.

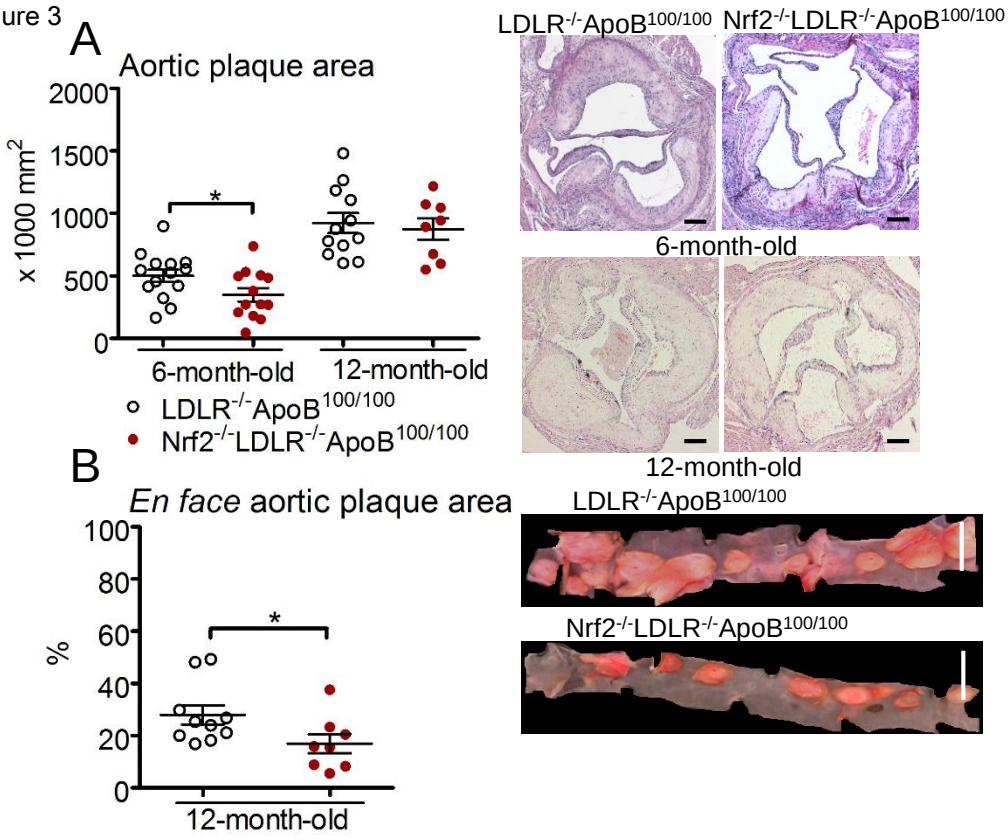

Figure 3. **Nrf2 deficiency impairs development of ageing-induced atherosclerosis in LDLR$^{-/-}$ApoB$^{100/100}$ female mice.** LDLR$^{-/-}$ApoB$^{100/100}$ (white dots) and Nrf2$^{-/-}$LDLR$^{-/-}$ApoB$^{100/100}$ female mice (red dots) were aged for 6 or 12 months on a chow diet. **A,** Quantification of cross-sectional lesion area (μm^2) from aortic root of LDLR$^{-/-}$ApoB$^{100/100}$ and Nrf2$^{-/-}$LDLR$^{-/-}$ApoB$^{100/100}$ female mice at the age of 6 or 12 months. Representative pictures of hematoxylin-eosin stained sections. **B,** Lesion coverage of descending aorta (%) by *en face* analysis of 12-month-old female mice. Representative pictures of aortic root are shown with a scale bar 100 μm and en face aortas with a scale bar of 1 mm. Each dot represents one mouse and the horizontal line represents mean ± SEM, *P<0.05 by Student's *t*-test. Number of mice analyzed: 6-month-old LDLR$^{-/-}$ApoB$^{100/100}$ n=14 and Nrf2$^{-/-}$LDLR$^{-/-}$ApoB$^{100/100}$ n=13, 12-month-old LDLR$^{-/-}$ApoB$^{100/100}$ n=10-12 and Nrf2$^{-/-}$LDLR$^{-/-}$ApoB$^{100/100}$ n=8.

Figure 4

FIG 4.

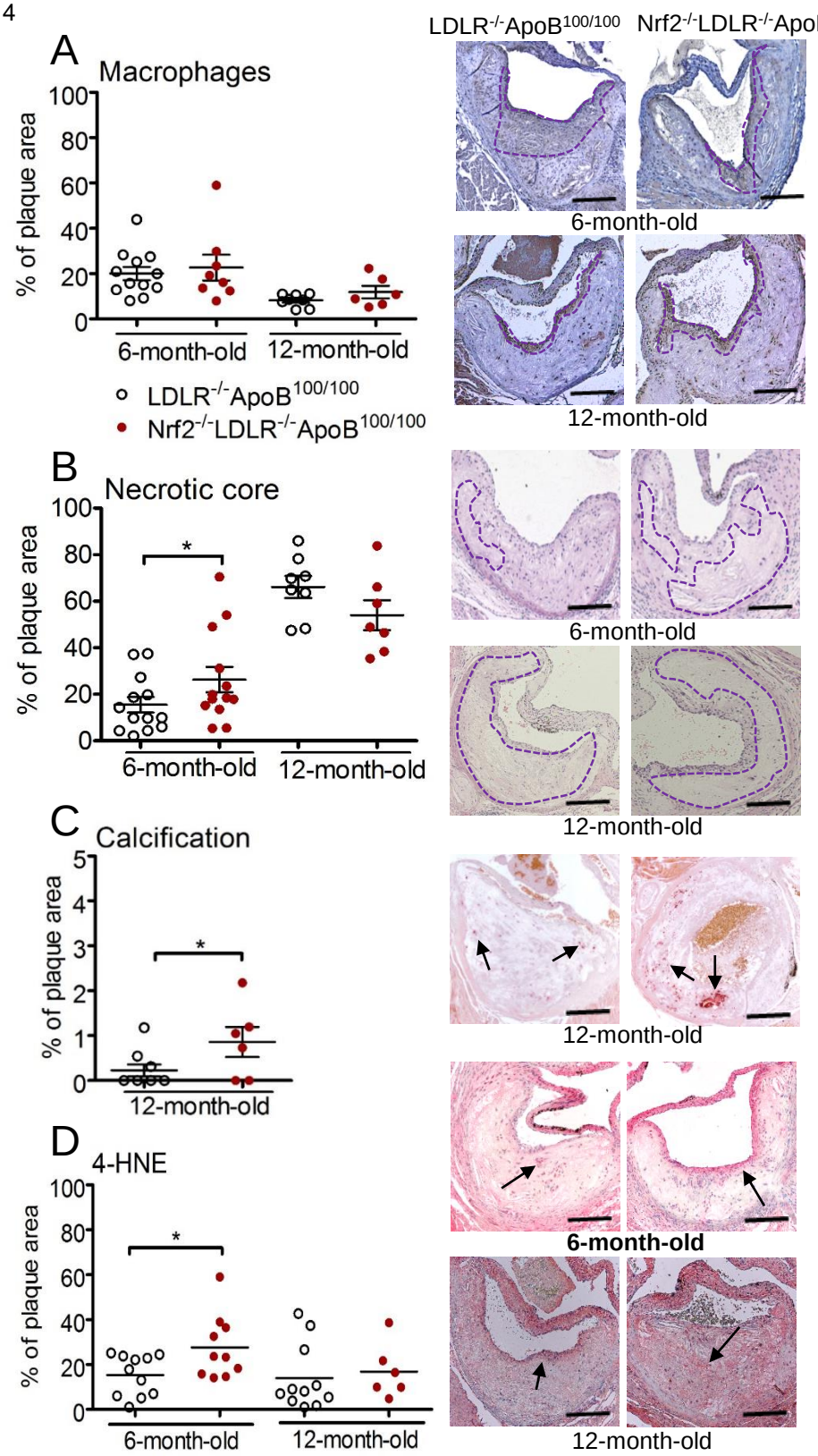

Figure 4. **Nrf2 deficiency promotes necrosis and calcification in fibroatheroma plaques in LDLR$^{-/-}$ApoB$^{100/100}$ female mice.** LDLR$^{-/-}$ApoB$^{100/100}$ (white dots) and Nrf2$^{-/-}$LDLR$^{-/-}$ApoB$^{100/100}$ female mice (red dots) were aged for 6 or 12 months on a chow diet. **A,** Lesion macrophage positive lesion area (outlined with a dotted line), **B**, necrotic area (hematoxylin-eosin staining, necrotic area outlined with a dotted line) **C**, plaque calcification (Alizarin Red S staining, black arrows depict red-stained calcifications) and **D**, 4-HNE positive lesion area measured in relation to total lesion area (%) in aortic root sections. Representative pictures are shown with a scale bar 100 μm. Each dot represents one mouse and the horizontal line represents mean ± SEM, *P<0.05, **P<0.01 by Student's *t*-test. Number of mice analyzed: 6-month-old LDLR$^{-/-}$ApoB$^{100/100}$ n=7-13 and Nrf2$^{-/-}$LDLR$^{-/-}$ApoB$^{100/100}$ n=6-12, 12-month-old LDLR$^{-/-}$ApoB$^{100/100}$ n=7-11 and Nrf2$^{-/-}$LDLR$^{-/-}$ApoB$^{100/100}$ n=6-7.

FIG 5.

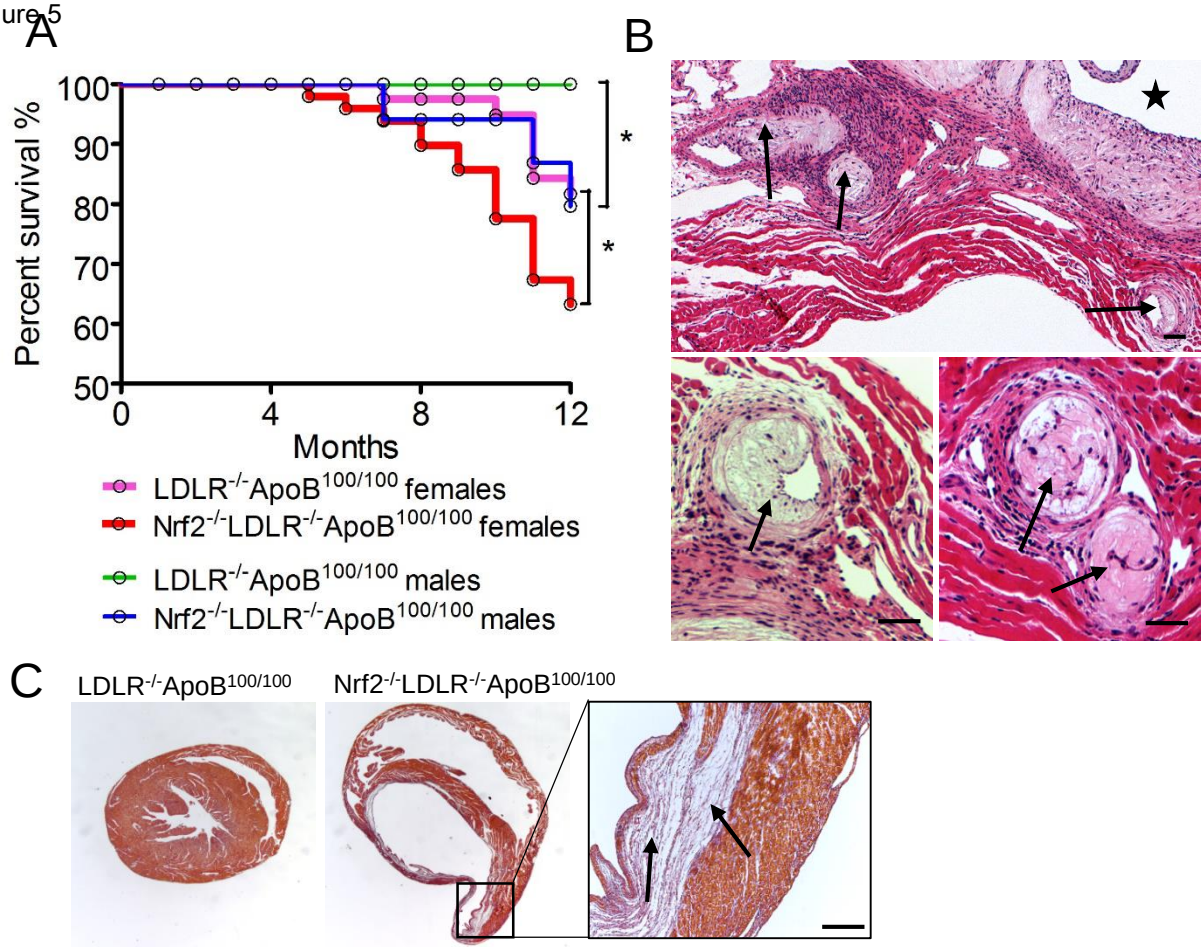

Figure 5. Nrf2 deficiency predisposes to myocardial infarction and sudden death in LDLR$^{-/-}$ApoB$^{100/100}$ female mice. A, Survival curve (%) of LDLR$^{-/-}$ApoB$^{100/100}$ (n=53) and Nrf2$^{-/-}$LDLR$^{-/-}$ApoB$^{100/100}$ (n=44) female and LDLR$^{-/-}$ApoB$^{100/100}$ (n=30) and Nrf2$^{-/-}$LDLR$^{-/-}$ApoB$^{100/100}$ (n=15) male mice until the age of 12 months, when mice were sacrificed for analysis. **B**, Representative pictures of hematoxylin-eosin stained coronary artery sections from Nrf2$^{-/-}$LDLR$^{-/-}$ApoB$^{100/100}$ female mice died of myocardial infarction at the age of 7 months. Coronary arteries are indicated by black arrows and aortic lumen by black star. **C**, Myocardium sections of Nrf2$^{-/-}$LDLR$^{-/-}$ApoB$^{100/100}$ female mice were stained with Masson Trichrome. Histopathological examination revealed regional fibrotic scar tissue formation (indicated by black arrows) in infarcted area. Representative pictures are shown with a scale bar 100 μm, statistical significance *P<0.05, **P<0.01 by Log-rank test.

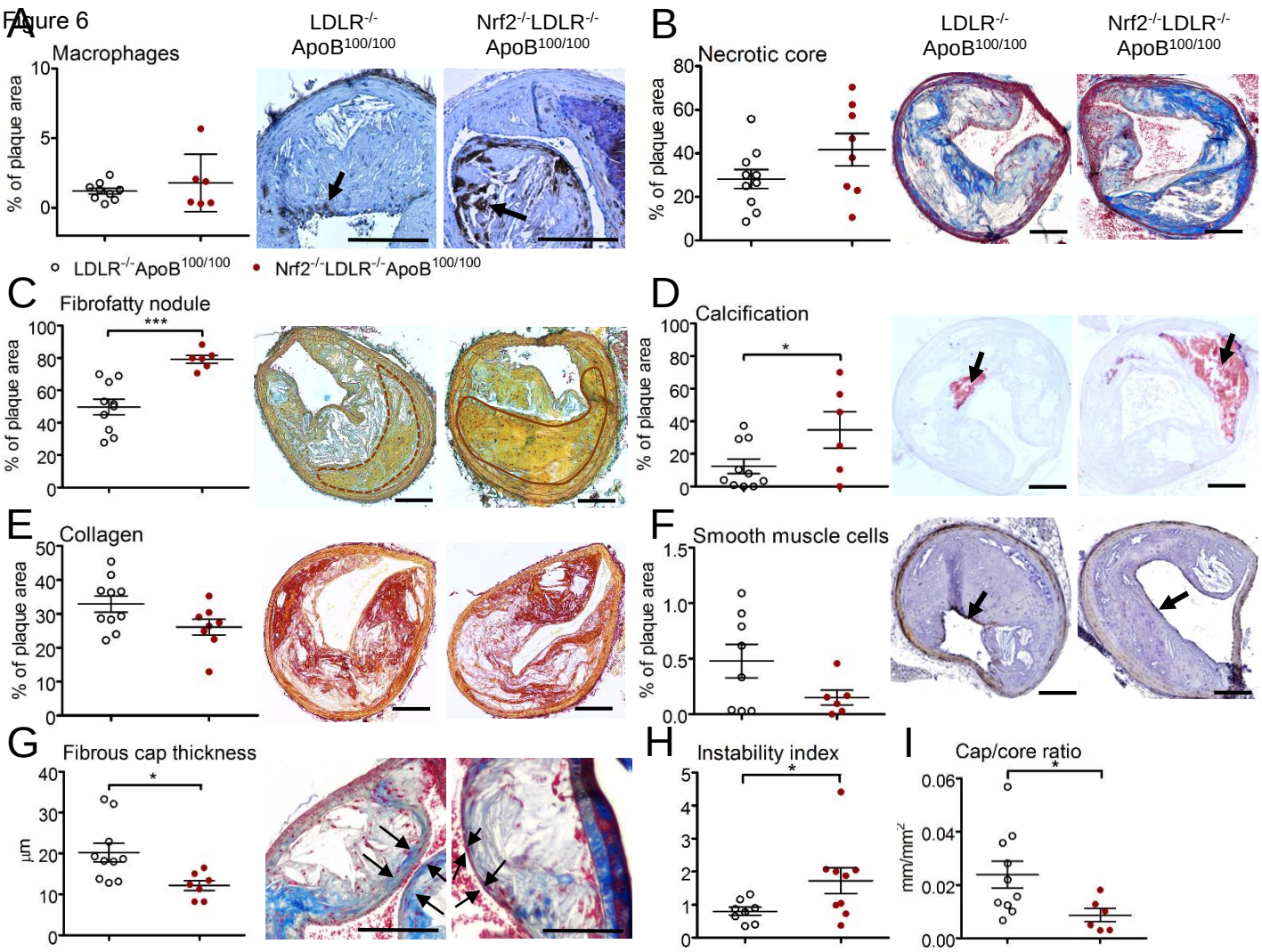

Figure 6. Nrf2 deficiency promotes plaque instability in brachiocephalic artery of aged LDLR$^{-/-}$ApoB$^{100/100}$ female mice. LDLR$^{-/-}$ApoB$^{100/100}$ (n=8-10) (white dots) and Nrf2$^{-/-}$LDLR$^{-/-}$ApoB$^{100/100}$ mice (n=6-9) (red dots) were sacrificed at the age of 12 months and plaque compositions was analysed from the brachiocephalic artery. Characteristics of instabile plaque, such as **A**, macrophage area stained with representative pictures of mMQ stained sections, **B**, Necrotic core area analysed from Masson Trichrome stained sections and **C**, fibro fatty nodule area (outlined with a dotted line) was analysed from Movat´s Pentachrome staining and all the quantifications were normalized to total lesion area, with representative pictures. **D**, Plaque calcification (%) was analysed from Alizarin Red S stained sections (black arrows depicit red-stained calcification) in relation to total lesion area with representative pictures. Characteristics of stabile plaque, such as **E**, plaque collagen content was evaluated from Picro Sirius Red staining and **F**, smooth muscle cell content from αSMA stained sections in relation to plaque area with representative pictures. Important hallmark of vulnerable plaque, **G**, a fibrous cap thickness (µm), was measured from Masson´s Trichrome stained sections, with representative pictures from thinned cap (indicated by black arrows). **H**, Plaque instability index and **I**, cap to core ratio were calculated as based on plaque morphological analysis, described more in detail in methods. Representative pictures are shown with a scale bar 100 µm. Each dot represents one mouse and the horizontal line represents mean ± SEM *P<0.05, * P<0.05, **P<0.01, ***P<0.001 by Student's *t*-test.

Figure 7

FIG 7.

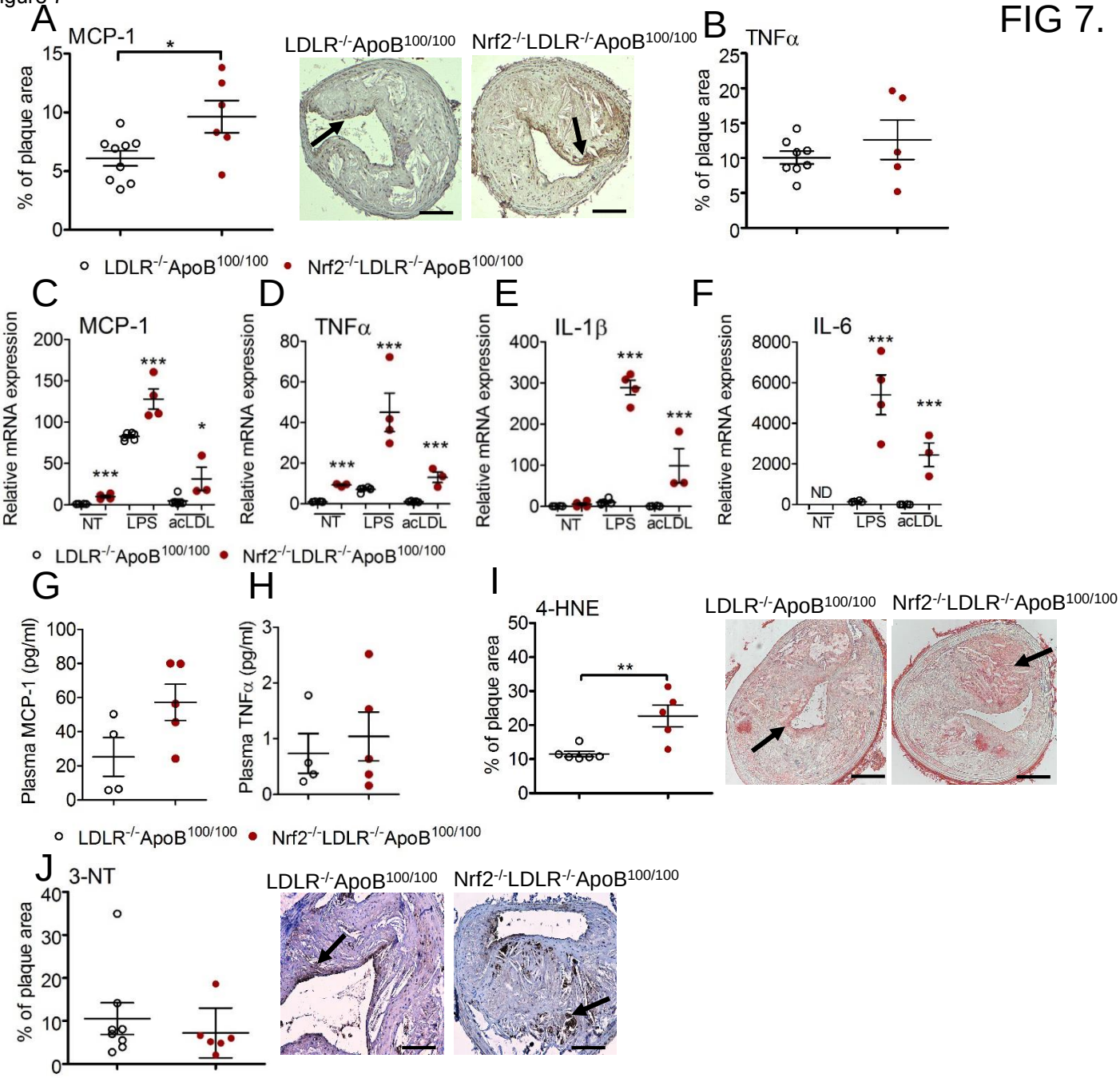

Figure 7. Nrf2 deficiency promotes inflammation and oxidative stress in atheroma plaque. LDLR$^{-/-}$ApoB$^{100/100}$ (n=6-9) (white dots) and Nrf2$^{-/-}$LDLR$^{-/-}$ApoB$^{100/100}$ mice (n=5-6) (red dots) were sacrificed at the age of 12 months and plaque inflammation was analysed from the brachiocephalic artery. Quantification of **A**, MCP-1 positive staining area (indicated by black arrows) in relation to plaque area with representative pictures, and **B**, TNFα positive staining area in relation to plaque area. LDLR$^{-/-}$ApoB$^{100/100}$ and Nrf2$^{-/-}$LDLR$^{-/-}$ApoB$^{100/100}$ bone marrow cells were isolated and differentiated to macrophages. mRNA expression of pro-inflammatory cytokines **C**, MCP-1, **D**, TNF-α, **E**, IL-1β and **F**, IL-6 were detected in basal conditions (n=4-6) and after treatment with AcLDL (n=3-6) or LPS (n=3-6) in bone marrow derived macrophages. Plasma **G**, MCP-1 and **H**, TNFα levels were measured from LDLR$^{-/-}$ApoB$^{100/100}$ (n=4) and Nrf2$^{-/-}$LDLR$^{-/-}$ApoB$^{100/100}$ mice (n=5). Plaque **I**, 4-HNE and **J**, 3-NT positive plaque area (%) (indicated by black arrows) normalized to total plaque area with representative sections. Representative pictures are shown with a scale bar 100 μm. Each dot represents one mouse and the horizontal line represents mean ± SEM, *P<0.05, **P<0.01, ***P<0.001 by Student's *t*-test.